AD-A183 509 POTENTIAL ENERGY SURFACES AND TRANSITION MOMENTS OF CL 1/1
ATOM IN XE SOLID M.. (U) STATE UNIV OF NEW YORK AT
BUFFALO DEPT OF CHEMISTRY I LAST ET AL. AUG 87
UNCLASSIFIED UBUFFALO/DC/87/TR-48 N00014-86-C-0043 F/G 7/2 NL

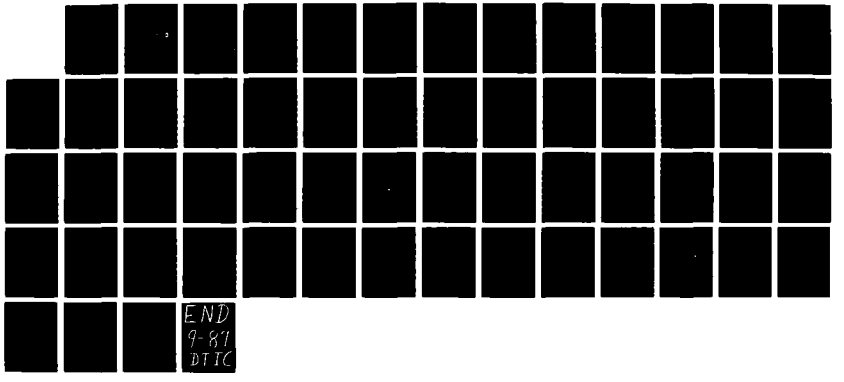

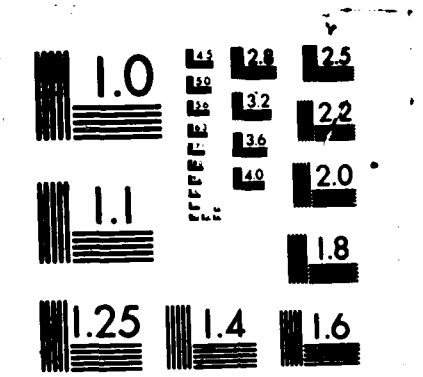

OFFICE OF NAVAL RESEARCH

Contract N00014-86-0043

TECHNICAL REPORT No. 48

Potential Energy Surfaces and Transition Moments of Cl Atom in Xe Solid Matrix

by

Isidore Last, Thomas F. George, Mario E. Fajardo and V. A. Apkarian

Prepared for Publication

in

Journal of Chemical Physics

Departments of Chemistry and Physics
State University of New York at buffalo
Buffalo, New York 14260

August 1987

UNCLASSIFIED

SECURITY CLASSIFICATION OF THIS PAGE

AD-A183589

REPORT DOCUMENTATION PAGE

1a. REPORT SECURITY CLASSIFICATION: Unclassified	1b. RESTRICTIVE MARKINGS
2a. SECURITY CLASSIFICATION AUTHORITY	3. DISTRIBUTION/AVAILABILITY OF REPORT: Approved for public release; distribution unlimited
2b. DECLASSIFICATION/DOWNGRADING SCHEDULE	
4. PERFORMING ORGANIZATION REPORT NUMBER(S): UBUFFALO/DC/87/TR-48	5. MONITORING ORGANIZATION REPORT NUMBER(S)
6a. NAME OF PERFORMING ORGANIZATION: Depts. Chemistry & Physics, State University of New York; 6b. OFFICE SYMBOL (If applicable)	7a. NAME OF MONITORING ORGANIZATION
6c. ADDRESS (City, State and ZIP Code): Fronczak Hall, Amherst Campus, Buffalo, New York 14260	7b. ADDRESS (City, State and ZIP Code): Chemistry Program, 800 N. Quincy Street, Arlington, Virginia 22217
8a. NAME OF FUNDING/SPONSORING ORGANIZATION: Office of Naval Research; 8b. OFFICE SYMBOL (If applicable)	9. PROCUREMENT INSTRUMENT IDENTIFICATION NUMBER: Contract N00014-86-K-0043
8c. ADDRESS (City, State and ZIP Code): Chemistry Program, 800 N. Quincy Street, Arlington, Virginia 22217	10. SOURCE OF FUNDING NOS. — PROGRAM ELEMENT NO. / PROJECT NO. / TASK NO. / WORK UNIT NO.

11. TITLE: Potential Energy Surfaces and Transition Moments of Cl Atom in Xe Solid Matrix

12. PERSONAL AUTHOR(S): Isidore Last, Thomas F. George, Mario E. Fajardo and V. A. Apkarian

13a. TYPE OF REPORT	13b. TIME COVERED FROM ____ TO ____	14. DATE OF REPORT (Yr., Mo., Day)	15. PAGE COUNT
		August 1987	51

16. SUPPLEMENTARY NOTATION: Prepared for publication in Journal of Chemical Physics

17. COSATI CODES: FIELD	GROUP	SUB. GR.

18. SUBJECT TERMS (Continue on reverse if necessary and identify by block number): Cl ATOM, IN SOLID, Chlorine, SEMIEMPIRICAL METHODS, POTENTIAL ENERGY SURFACES, SUBSTITUTIONAL TRAPPING SITES, TRANSITION MOMENTS, $Xe_2^+Cl^-$ STABILITY, Xenon Chlorine

19. ABSTRACT (Continue on reverse if necessary and identify by block number)

Xe solid containing a Cl atom is considered by the semiempirical diatomics-in-ionic-systems method which takes into account the charge delocalization in an ionic state and the coupling between the neutral and ionic states. The calculation shows that the Cl atom has motional freedom in substitutional trapping sites which leads to the broadening of absorption bands. The vertically accessed ionic states are treated as $Xe_{12}^{+n}Cl_L^-$ molecules with a nonuniform positive charge distribution. The most stable ionic complex has the $Xe_2^+Cl_L^-$ molecular configuration. Cl atoms at interstitial sites are treated as Xe_6^+Cl molecules with $Xe_6^+Cl_L^-$ excited states. The results of the calculation are in general agreement with recent experiments.

20. DISTRIBUTION/AVAILABILITY OF ABSTRACT	21. ABSTRACT SECURITY CLASSIFICATION
UNCLASSIFIED/UNLIMITED ☒ SAME AS RPT. ☒ DTIC USERS ☐	Unclassified

22a. NAME OF RESPONSIBLE INDIVIDUAL	22b. TELEPHONE NUMBER (Include Area Code)	22c. OFFICE SYMBOL
Dr. David L. Nelson	(202) 696-4410	

DD FORM 1473, 83 APR — EDITION OF 1 JAN 73 IS OBSOLETE.

UNCLASSIFIED

SECURITY CLASSIFICATION OF THIS PAGE

Journal of Chemical Physics, in press

Potential Energy Surfaces and Transition Moments of Cl Atom in Xe Solid Matrix

Isidore Last* and Thomas F. George
Departments of Chemistry and Physics & Astronomy
239 Fronczak Hall
State University of New York at Buffalo
Buffalo, New York 14260

and

Mario E. Fajardo and V. A. Apkarian
Department of Chemistry
University of California
Irvine, California 92717

Abstract

Xe solid containing a Cl atom is considered by the semiempirical diatomics-in-ionic-systems method which takes into account the charge delocalization in an ionic state and the coupling between the neutral and ionic states. The calculation shows that the Cl atom has motional freedom in substitutional trapping sites which leads to the broadening of absorption bands. The vertically accessed ionic states are treated as $Xe_{12}^{+}Cl^{-}$ molecules with a nonuniform positive charge distribution. The most stable ionic complex has the $Xe_2^{+}Cl^{-}$ molecular configuration. Cl atoms at interstitial sites are treated as Xe_6Cl molecules with $Xe_6^{+}Cl^{-}$ excited states. The results of the calculation are in general agreement with recent experiments.

*Permanent address: Soreq Nuclear Research Center, Yavne 70600, Israel

1. Introduction

Rare-gas solids containing halogen molecules demonstrate interesting spectroscopic properties when exposed to laser radiation.[1-5] These properties are associated with the formation of quasistable ionic rare-gas-halogen molecules. The same processes can also be observed in gas[6-11] and liquid phase[12,13] rare-gas-halogen mixtures.

The formation of the ionic rare-gas-halogen molecules was investigated in detail in Ref. 1 for solid xenon initially doped with Cl_2 and HCl molecules. Near-UV laser irradiation of the doped solid results in emission from the quasistable ionic molecules. In pure xenon hosts, $Xe_2^+Cl^-$ is responsible for this emission, whereas in mixed rare gas hosts, such as HCl:Xe:Ar or HCl:Xe:Kr (1:4:100), both Xe^+Cl^- and $Xe_2^+Cl^-$ are observed. The identity of the $Xe_2^+Cl^-$ emitter in condensed media was further verified in experiments that continuously spanned the three phases -- gas, liquid and solid.[13] The theoretical consideration of the ionic xenon-chlorine molecules in Xe solid also confirmed that the observed emission is associated with the $Xe_2^+Cl^-$ molecule.[14] In Xe solid doped with HCl or Cl_2 molecules, there are several processes which lead to the formation of the $Xe_2^+Cl^-$ molecule.[1] Two-photon cooperative absorption was established as the main mechanism in the case of HCl-doped solids.[1] The quantum electrodynamic formalism of two-photon cooperative absorption and its efficiency in condensed media has previously been discussed.[15] In the case of Cl_2-doped solids, sequential two-photon absorption could not be ruled out.[1] In this mechanism the first photon dissociates the Cl_2 molecule and forms two Cl atoms, and the second photon transfers an electron from the Xe matrix to the Cl atom to form an activated complex which relaxes to the quasistable $Xe_2^+Cl^-$ molecule. In either scheme, the end result is the permanent dissociation of

Cl_2 and the creation of solids doped with atomic chlorine. The subsequent spectroscopy is conducted at low intensities such that two-photon processes are diminished. The states probed in this weak-field limit then refer to those of Cl atoms isolated in rare-gas matrices.

The processes in the rare-gas solids doped by halogen molecules and exposed to laser radiation are complicated and involve several problems which can be separately studied theoretically. We shall mention here the most important of these problems: a) motion and equilibrium localizations of halogen molecules in the host matrix; b) excitation by photons of the electronic states of the halogen molecules inside the host matrix; c) excitation by photons of the electronic states with the transfer of an electron from the host matrix to the halogen molecule; d) cage effect on the dissociation of the electronically excited halogen molecules and ions (Cl_2^* and Cl_2^-, for example); e) motion and equilibrium localizations of halogen atoms in the host matrix; f) excitation by photons of the electronic states with a transfer of an electron from the host matrix to the halogen atom. g) relaxation of atoms after the electron transfer and the formation of quasistable ionic rare-gas-halogen molecules; h) spectroscopic properties of the ionic rare gas-halogen molecules in the rare-gas matrix.

The unambiguous interpretation of experimental data, in particular excitation spectra, requires an understanding of the initial Cl atom site distributions. These are determined by the photodissociation dynamics and subsequent atomic motions as alluded to in (d) and (f) above. Reliable potential energy surfaces are crucial for such studies. The last problem (h) for the molecule $Xe_2^+Cl^-$ was considered in Ref. 14 within the framework of a relatively simple model. In this model, any exchange interactions between the $Xe_2^+Cl^-$ atoms and the matrix Xe atoms were neglected as well as

the coupling of the ionic $Xe_2^+Cl^-$ state with neutral Xe_2Cl electronic states. The geometry of the ionic $Xe_2^+Cl^-$ molecule in the solid was assumed to be the same as in the gas phase. The shift of the $Xe_2^+Cl^-$ emission wavelength in the solid matrix in comparison with that in the gas phase was found to be equal to -0.26 eV, not far from the experimental value of -0.38 eV. In Ref. 14 the problems (e) and (f) were also considered in order to estimate the activation energy of the ionic state formation.

The consideration of most of the problems cited above needs potential energy surfaces (PES) of the system, which can be calculated by the semiempirical diatomics-in-ionic-systems (DIIS) method.[16] This method will be used in this paper for the PES and transition moment calculations of a Cl atom inside an Xe cage (problems (e) and (f)) and the calculation of the structure of the quasistable rare-gas-halogen ionic molecules and spectroscopic transitions in these molecules (problems (g) and (h)). We shall then report some of the experimental findings and compare them to the theoretical results to establish the validity of the present approach.

2. The Diatomic-in-Ionic Systems (DIIS) Method

The semiempirical DIIS method[16] is designed for the calculation of polyatomic rare-gas-halogen systems R_nX consisting of an arbitrary number of rare-gas atoms R and one halogen atom X. The method takes into account the coupling between ionic and neutral electronic states and the positive charge delocalization between the rare gas atoms. The wave function Φ of the R_nX system is given as the linear combination

$$\Phi = \sum_{i=1}^{J} \sum_{m=1}^{3} C_{im} \Phi_{im}, \qquad (1)$$

where $J = n + 1$ is the number of atoms in the system, ϕ_{im} are polyatomic wave functions which describe diabatic states with fixed electronic configuration of the atoms, and m is the index of the orientation of a P-symmetry atomic wave function. The main feature of the R_nX system is that in any electronic configuration one atom only has the electron shell of P-symmetry whereas all other atoms have closed electron shells of spherical (S) symmetry. In neutral configurations the halogen atom has a P-symmetry wave function. In ionic configurations a positive rare-gas ion R_i^+ has a P-symmetry wave function; all other (neutral) rare-gas atoms R_j $(j \neq i)$ and the negative halogen ion X^- have S-symmetry electron shells. Describing the electronic configurations by the localization of the positive charge and by the orientation of the P-symmetry atomic wave function, we do not take into account, at least directly, the spin-orbit coupling. However, the shift of the levels due to the spin-orbit coupling can be accounted for indirectly by the proper choice of diatomic potentials.

The zero overlap of atomic orbitals (ZOAO) approximation, which is common in semiempirical methods, allows us to write any diabatic polyatomic function as a product of atomic group functions,

$$\phi_{im} = \chi_{im} \prod_{j(\neq i)} \chi_j \ , \qquad i = 1,2...J, \quad m = 1,2,3 \qquad (2)$$

where the P-symmetry group function χ_{im} describes either the neutral X atom or an ion R_i^+, and the group functions of S-symmetry χ_j $(j \neq i)$ describe neutral rare-gas atoms R_j and a halogen ion X^-. The 3J diabatic wave functions (2) form a polyatomic basis and produce the 3J×3J Hamiltonian matrix. This matrix determines the eigenstates and eigenvalues of the

adiabatic wave function (1), which describes an electronic state as a mixture of the neutral and ionic configurations.

The DIIS matrix elements are expressed in terms of the potentials of diatomic fragments of the system, except for the off-diagonal matrix elements which are responsible for the coupling between the ionic and neutral electronic configurations. These matrix elements (coupling terms) are considered as semiempirical parameters which fit known empirical or ab initio rare-gas-halogen diatomic data, other than potentials. In Ref. 16, where the Xe_nCl systems were calculated, the coupling terms were determined by fitting the transition moments between the ionic and neutral XeCl states. These coupling terms will be used in the present calculation. The diatomic potentials of the Xe_nCl fragments, namely Xe-Cl, $Xe\text{-}Cl^-$, Xe-Xe and $(Xe\text{-}Xe)^+$, will also be taken from Ref. 16, where they were obtained mostly by fitting empirical potentials.

3. Cl Atom in a Substitutional Site

Let us consider a Cl atom which replaces an Xe atom in the Xe solid matrix and is located inside a cage formed by 12 Xe atoms. These 12 Xe atoms are considered together with the Cl atom as a $Xe_{12}Cl$ molecule, whereas all other Xe atoms of the solid form a rigid matrix. The $Xe_{12}Cl$ molecule is calculated by the DIIS method, which takes into account the electron delocalization between the atoms of the molecule but neglects any exchange interaction and electron transfer between the $Xe_{12}Cl$ atoms and the Xe atoms of the matrix. Consequently, the energy of the system can be presented as a sum of the $Xe_{12}Cl$ energy (E_A), the matrix energy (E_M) and the energy of molecule-matrix interaction. In an ionic state the $Xe_{12}Cl$ molecule has, generally speaking, a dipole moment which polarizes the Xe atoms of the matrix. Consequently, the energy of the molecule-matrix interaction is

expressed as a sum of the polarization energy ε_p and the energy of the non-polarization components of the pairwise interactions $\bar{U}_{ij}$ between all atoms of the $Xe_{12}Cl$ molecule and the Xe atoms of the matrix,[14]

$$E = E_A + E_M + \sum_i \sum_j \bar{U}_{ij} + \varepsilon_p \quad , \tag{3}$$

where i and j are atomic indices of the molecule and the matrix, respectively. In the dipole approximation the polarization component of the interaction between the i-th ion (Xe^+ or Cl^-) and the j-th atom of the matrix is

$$\varepsilon_{ij} = - \frac{e^2 \alpha_j}{2R_{ij}^4} \quad , \tag{4}$$

where α_j is the Xe atom polarizability and R_{ij} is the interatomic distance. Excluding ε_{ij} from the empirical of <u>ab initio</u> potential U_{ij}, one obtains the non-polarization component

$$\bar{U}_{ij} = U_{ij} - \varepsilon_{ij} \quad . \tag{5}$$

The higher-order multiple interactions are incorporated in the U_{ij} term. If the i-th atom of the Xe_{12} Cl molecule is neutral, then the polarization is zero ($\varepsilon_{ij} = 0$) and $\bar{U}_{ij}$ coincides with U_{ij}. In the neutral $Xe_{12}Cl$ configuration all $\bar{U}_{ij}$ coincide with U_{ij} and $\varepsilon_p = 0$ in Eq. (3). The diatomic potentials $\bar{U}_{ij}$ or U_{ij} are taken from Ref. 16 where they are expressed analytically. In the present calculation, 66 matrix atoms are taken into account in the pairwise interactions in Eq. (3). In an ionic $Xe_{12}^+Cl^-$

configuration the polarization energy ϵ_p of the system is determined as a sum of the polarization energy of these 66 atoms, including their dipole-dipole interaction, and the polarization energy of the matrix which is considered as a continuum.[14]

Since the $Xe_{12}Cl$ molecule consists of 13 atoms, the order of the Hamiltonian matrix is 39×39 and the number of electronic states is 39. While any given state includes, generally speaking, both ionic and neutral electronic configurations, one of these two configurations is always predominant. We shall designate the states according to their predominant configuration. For example, a largely ionic state will be called an ionic state. In the $Xe_{12}Cl$ molecule, only three states are neutral and 36 states are ionic.

A. Ground State PES

As shown by simple calculations in Refs. 1 and 14, the Cl atom has some freedom of motion inside the Xe cage. This finding is confirmed by the present more complicated DIIS calculation. When the Cl atom is located in the center of the cage and the $Xe_{12}Cl$ molecule is symmetric, the minimum energy is obtained for the cage slightly shrinked, with the Xe-Cl distance of 4.33 Å, as compared to 4.4 Å in the undeformed matrix. The ground state PES is obtained for a fixed location of the Xe atoms, with the distance to the center of the cage of 4.33 Å regardless of the Cl location. The shift of the Cl atom from the center of the cage is described by spherical coordinates (R,θ,ϕ) shown in Fig. 1. The angular and Cartesian coordinates of the Xe atoms are presented in Table 1.

The PES are presented in Fig. 2 for four different planes, each with a fixed ϕ angle. The energy in the center ($R = 0$) is -3.4485 eV. The shape of the PES is different for different values of ϕ, but the general feature

is the presence of the relatively broad region of almost constant potential with the variations within the range of 1 meV. Twelve very shallow potential wells are shifted by 0.5-0.8 Å from the cage center toward the Xe atoms. The energy minimum of -3.4495 eV is located at the point R = 0.65 Å. The potential wells are separated one from another by low barriers of 0.5 meV.

Even at absolute zero temperature, the Cl atom cannot be located in a well due to the quantal motion. The uncertainty principle gives approximately 0.4 meV for the energy of the Cl atom in a well, which is enough for Cl to tunnel between the wells. The thermal energy exceeds the quantal energy and consequently increases the attainable region at ~ 5 K. This expansion of the region of the Cl motion leads first to a decrease of the average distance $\bar{R}$ to the cage center since the Cl atom at T > 5 K can reach the central part of the cage. Further increase in the temperature leads to a slight increase of the average distance of the Cl atom from the cage center (Fig. 3). The $\bar{R}$ minimum is located at 10 K. If we take into account the quantal motion, then the average radius $\bar{R}$ will be smaller for very low temperatures $T \leq 5K$ and the minimum will not be as well defined as in Fig. 3.

B. Influence of the Xe Atoms Shift on the Ground State Energy

The previous consideration was restricted to the case of a rigid Xe cage with Cl atom moving inside it. However, the Xe atoms can also be shifted, first because of their vibrational motion and second because of their interaction with the Cl atom. In order to check how the shift of the cage atoms affects the energy, the minimum energy geometry was calculated for a fixed location of the Cl atom and for a cage with one Xe atom shifted from the symmetrical position (R_{Xe} = 4.33 Å) along the radius. All other 11

cage Xe atoms are fixed in the symmetrical position. According to the results of the calculation at low temperatures T < 20 K, when the accessible region is approximately restricted to energies less than -3.447 eV (Fig. 2), the shift of a Xe atom can lower the energy by not more than 1 meV. At the minimum energy points (R = 0.65 Å, θ = 45°, ϕ = 0°, see Fig. 2a), the shift of a Xe atom stabilizes the system by lowering the energy to -3.4505 eV. However, it is unlikely that the Xe atoms can relax to trap the Cl atom in a well, as the phonon energy is higher than 1 meV. At higher temperatures the Cl atom reaches the regions associated with a stronger perturbation of the nearest Xe atom location. However, the energy of this perturbaton is still smaller than the thermal energy. The changes of the transition energies and transition moments due to the vibrational motion of Xe atoms are small and can be neglected.

C. Ionic States

We consider now the PES for ionic states. As for the ground state case, the PES are expressed as functions of the Cl spherical coordinates, suggesting the Xe atoms to be fixed. The potential energy curves of all 36 ionic states along the line running from the cage center to one of the nearest Xe atoms (i = 2, θ = 45°, ϕ = 0°, for example) are presented in Fig. 4. This line is of primary interest since it crosses the minimum energy well in the ground state (Fig. 2a). The energy of the ionic states is given in Fig. 4 relative to the ground state energy for the central (R = 0) position of the Cl atom. The potential curves form a complicated system of intersecting lines with only the lowest ionic state, k = 4, being separated from the others. Most of the intersections in Fig. 4 are real (not avoided) crossings, since the states with crossings have different symmetry with respect to the considered direction which is the symmetry axis of the

crystal. Most of the diabatic curves each have a shallow minimum in the interval 1-1.2 Å.

The potential curves for a fixed radius R = 1.1 Å and changing angles θ and ϕ are presented in Fig. 5 for the twelve lowest ionic states k = 4-15. The potential curves in Fig. 5a are located in a plane which includes the line $\theta = 45°$, $\phi = 0°$ passing through the i = 2 Xe atom (the potentials along this line are presented in Fig. 4) and the line $\theta = 65.905°$, $\phi = 26.565°$ passing between two Xe atoms, i = 1 and 2 (Table 1, Fig. 1). Just the last line leads to the formation of the quasistable $Xe_2^+Cl^-$ molecule, which will be considered later. The potential curves in Fig. 5b are presented for a fixed angle $\theta = 90°$ and the ϕ angle changing from 0° to 45°. The point $\phi = 45°$ on the abscissa coincides with the direction to the Xe atom i = 1 (Table 1, Fig. 1). In contrast to the potential curves in Fig. 4, the potential curves presented in Fig. 5 demonstrate mostly avoided crossings. Some of the avoided crossings have very small splitting of the order of 0.01 - 0.02 eV which are difficult to detect in the figures. The lowest potential curve k = 4 in Fig. 5 is also separated from other curves, as in the case presented in Fig. 4. The adiabatic ionic states are denoted here by numbers, according to their energy, as it is difficult to denote them by symmetry, mainly because of the numerous crossings of the diabatic levels. A diabatic symmetry can be associated with the k = 4 state, which corresponds to the $4^2\Gamma$ state in the asymptotic Xe_2Cl case.

The PES of the two lowest ionic states k = 4 and 5, are presented in Fig. 6 for the plane $\phi = 0°$. The ground state PES for this plane is presented in Fig. 2a. The PES of the k = 4 and k = 5 states are similar to each other. Each of these PES has a minimum located on the x-axis which is equidistant to four Xe atoms (i = 1,2,7,8, Table 1). The location of these

minima differ significantly from those of the ground state which are located on a line passing through a Xe atom (Fig. 2a).

D. Excitation of the System to Ionic States

In order to study the excitation of the sytem by photons, one needs the energy of transitions and the transiton moments between the ground and excited states as a function of the Cl atom location (R,θ,ϕ). We are interested in the excitation from the neutral ($k = 1,2,3$) to the ionic ($k \geq 4$) states. The three lowest (neutral) states are degenerate at the center of the cage ($R = 0$) and nearly degenerate in the vicinity of it ($R \leq 0.4$ Å), so that the population of the first two excited states is equal or comparable to the ground state population. Taking into account this possibility, we have to consider the excitation to ionic states from all three neutral states, at least in the region around the cage center.

The excitation energy from a neutral k_1 to an ionic k_2 state,

$$V_{k_1k_2} = E_{k_2} - E_{k_1}, \tag{6}$$

depends on the location of the Cl atom inside the cage and therefore is a function of the coordinates R,θ,ϕ. The probability of the $k_1 \rightarrow k_2$ excitation for the Cl atom located in a small volume Δv about the point R,θ,ϕ is proportional to the probability $\frac{dW_{k_1}}{dv}\Delta v$ of the Cl location in this volume when the system is in the initial k_1 state, and to the square of the transition moment $M^2_{k_1k_2}$:

$$\Delta Q_{k_1k_2} = M^2_{k_1k_2}\frac{dW_{k_1}}{dv}\Delta v. \tag{7}$$

The value Q can be presented in arbitrary units as it shows only the relative contribution of different transitions and different Cl atom locations to the light absorption. If the quantal motion of the Cl atom is neglected and the thermal motion only is taken into account, then the probability density is expressed in terms of the Boltzmann distribution,

$$\frac{dW_{k_1}}{dv} = A \exp[-(E_{k_1} - E_0)/kT], \qquad (8)$$

where kT is the thermal energy, E_0 = -3.4495eV is the minimal energy (Fig. 2), and A is the normalization coefficient. The transition energy distribution is calculated here by a boxing procedure, whereby the accessible space for the Cl atom inside the cage is divided into small volumes Δv_j whose centers form a grid of points $R_j\theta_j\phi$ with transition energies V_j (for certain $k_1 \to k_2$). The energy scale is divided on small equal intervals ΔV (ΔV = 0.1 eV in this calculation) with energies V_i in the centers of these intervals. The relative probability Q_i of the excitation with the transition energy V_i is found by summing $\Delta Q_{k_1 k_2}$ (6) values of all volumes Δv_j whose transition energies V_j lie in the interval

$$V_i - \Delta V/2 \leq V_j \leq V_i + \Delta V/2 \quad . \qquad (9)$$

The transition energy distributions were obtained for the temperatures T = 5 K, 10 K, 20 K, 40 K, 80 K, 160 K. The distribution for T = 10 K and T = 80 K are presented in Figs. 7a and 7b, respectively. The figures demonstrate the total distributions and the distributions to three individual ionic states, namely to the lowest one k_2 = 4 and to two higher states, k_2 = 5 and 20, with a strong absorption. The distributions for 10 K and 80 K do not

differ significantly from one another, leading us to the conclusion that the thermal motion does not affect the absorption to any significant extent. Both distributions have two maxima which are separated by a deep minimum. The maxima and the lower limit of the absorption are shifted slightly to smaller energies when the temperature increases. This shift is due to the expansion of the accessible area to the regions where the transition energies are smaller than in the central region.

The strongest transition at both temperatures is $1 \rightarrow 5$, i.e., from the ground state to the second ionic state. The $1 \rightarrow 5$ transition moments fall mainly within the limits 0.9 - 1.7 D. The excitation to the first ionic state, $k = 4$, is relatively insignificant. The excitation to the third ionic state, $k = 6$ (not shown in Fig. 7), becomes important only at the higher temperature of 80 K. This increase in absorption is due to the regions with $R > 1$ Å which are accessible for higher temperatures only. In these regions the $1 \rightarrow 6$ transition moment is large, about 2.1 D, but the transition energy is relatively low so that the $k = 6$ absorption maximum has lower energy than the maximum of the absorption to the $k = 5$ state (Fig. 7b). In all other cases the energy of the absorption maximum increases with the state index k.

The results presented in Fig. 7 show that due to inhomogeneous broadening, the absorption forms a wide band in the range 3.5-4.7 eV, roughly, which grows weak in the middle. The total absorption cross section (in arbitrary units) is shown in Fig. 3, which is seen to increase slightly with temperature.

E. Formation of Quasistable Ionic Molecules

After the excitation of the system to an ionic state and the formation of an activated complex,[14] the atoms begin their shift to a new equilibrium

geometry. This relaxation of the system is associated with the redistribution of the positive charge of the Xe atoms. The charge distribution in the activated complex depends significantly on the location of the Cl atom. When the Cl atom is located in the central region of the cage, then the charge is generally shared by several Xe atoms in such a way that none of the atoms can individually carry an important part of the charge. The statistical consideration of the activated complexes shows that inside the region $R < 0.7$ Å there are no cases with one atom carrying more than half of the charge, and only in 30% of the cases does one atom carry more than 0.4 of the charge. When the Cl atom is located far from the cage center ($R > 0.7$ Å), then the charge is transferred by the excitation mostly to one of the Xe atoms, but even in these cases more than 30% of the charge is always distributed among several other Xe atoms. These distant locations do not contribute much to the absorption, at least at low temperatures. At 10 K, for example, only in 12% of the activated complexes are there Xe atoms which carry more than half of the charge. Furthermore, there are not many cases where the charge is distributed mainly between two atoms. These statistics demonstrate that the activated complexes are neither $Xe^{+}Cl^{-}$ nor $Xe_2^{+}Cl^{-}$ molecules. They have to be considered as $Xe_{12}^{+}Cl^{-}$ molecules with various positive charge distributions among the twelve Xe atoms.

In contrast to the activated complexes, the positive charge of the most stable ionic system is found to be localized mostly on two Xe atoms forming a $Xe_2^{+}Cl^{-}$ molecule inside the Xe matrix. This finding substantiates the suggestions made in Refs. 1 and 14. The relaxation from activated complexes in different ionic states to the equilibrium geometry of the lowest ($k = 4$) ionic state is possible due to the crossings of the PES demonstrated in Figs. 4 and 5 for fixed Xe atoms. The relaxation of the

system involves obviously also the charged Xe atoms. The shift of Xe atoms increases the possibility of crossings between the states including, probably, the lowest (k = 4) state which is separated from other states when the Xe atoms are fixed.

In order to find the equilibrium geometry of the lowest ionic (k = 4) state, the calculations were performed for different $Xe_{12}^{+}Cl^{-}$ configurations. Varying the locations of all 13 atoms in these configurations, we selected only those directions of the atomic shifts which lead to the energy decrease. The calculations of additional configurations show that there is one only minimum energy configuration which gives the equilibrium geometry. At this equilibrium geometry the Cl^{-} ion is shifted from the center of the cage by 1.12 Å, forming with two Xe atoms (i = 1,2) the $Xe_2^{+}Cl^{-}$ molecule. The molecule has the shape of an isosceles triangle with the Xe-Cl-Xe angle as 60.2°, each Xe-Cl distance as 3.30 Å, and the Xe-Xe distance as 3.31 Å. This geometry does not differ much from the gas-phase $Xe_2^{+}Cl^{-}$ geometry in the $4^2\Gamma$ state.[16-18] The comparison with the results obtained in Ref. 16 by the same method and with the same semiempirical parameters as in the present calculation shows that the solid matrix extends slightly, by 0.06-0.07 Å, the interatomic distances in the $Xe_2^{+}Cl^{-}$ molecule. The ionic charge of the Cl atom is -0.97e, almost the same as in the gas-phase molecule (-0.964e).[16] The positive charge is partly delocalized so that the common charge of the two Xe atoms of the $Xe_2^{+}Cl^{-}$ molecule is +0.932e, whereas +0.038e of the charge is distributed between the other ten Xe atoms. One of these atoms (i = 3) carries most of this charge, +0.021e. The symmetry axis of the $Xe_2^{+}Cl^{-}$ molecule is located in a plane formed by the x-axis and the diagonal line of the yz-plane. The coordinates of the Cl atom and two Xe atoms (i = 1,2) of the $Xe_2^{+}Cl^{-}$ molecule are shown in Table 2. The Xe atom i = 3 which carries

some charge (0.02|e|) is shifted further from the Cl atom by 0.1 Å. Its coordinates are also shown in Table 2. All other Xe atoms are located at the same points as in the neutral state (Table 1).

As in the gas phase, the dominant transition from the ionic $4^2\Gamma$ state of the $Xe_2^+Cl^-$ molecule is to the $1^2\Gamma$ ground state with the large transition moment of 2.41 D. The transition energy from the $Xe_2^+Cl^-$ equilibrium geometry is $V_{4\to1}$ = 2.35 eV. This value is smaller by 0.21 eV than the gas-phase transition energy, calculated in Ref. 16 with the same semiempirical parameters as here. The experimental value for the shift of the $Xe_2^+Cl^-$ transition energy in the solid is larger, 0.38 eV.[1] The simple model calculation of Ref. 14 gave 0.26 eV for the shift of the transition energy in the solid, which is closer to the experimental value. It is not surprising that the present, more sophisticated calculation gives for the transition energy shift a worse result than the simple model calculation.[14] In the model calculation the shift was estimated directly, whereas in the present calculation it is determined as the difference between the transition energies of two different systems, namely Xe_2Cl in the gas phase and $Xe_{12}Cl$ in the solid.

The potential curves for the inner deformation of the $Xe_2^+Cl^-$ molecule are presented in Fig. 8. These potential curves allow us to calculate the vibrational energy of the molecule. In the harmonic approximation the energy of the vibrational excitation is found to be equal to 0.034 eV along the molecular symmetry axis (Fig. 8a) and 0.012 eV along the Xe-Xe line (Fig. 8b). The vibrational ground state (v = 0) energies are 0.017 and 0.006 eV, respectively. If the system is in thermal equilibrium and the temperature is not higher than ~80 K, then only the ground state is of importance. Its vibrational motion broadens significantly the transition

energy to the repulsive electronic ground state k = 1, whose potential curves are shown in Fig. 8, as well. The estimations yield for the transition band width the values ΔV = 0.28 eV and 0.20 eV for the cases presented in Fig. 8a and 8b, respectively.

The potential curves of the translational motion of the $Xe_2^+Cl^-$ molecule inside the solid matrix are presented in Fig. 9. The potential wells are relatively shallow for all three mutual perpendicular directions of the translation shown in Fig. 9. The ground state (k = 1) potential curves are presented in Fig. 9 for the Xe_2Cl geometry coinciding with the equilibrium $Xe_2^+Cl^-$ geometry. In common with the potential curves for the $Xe_2^+Cl^-$ (k = 4) molecule, the k = 1 curves demonstrate minima whose locations coincide exactly (Fig. 9c) or roughly (Fig. 9a,b) with the k = 4 minima locations. The k = 1 minima are slightly deeper than the ionic k = 4 minima. It is important, however, to note that the ground state minima in Fig. 9 do not indicate any equilibrium configuration since the ground state potentials, in contrast to the ionic k = 4 potentials, are repulsive along the inner Xe_2Cl coordinates (Fig. 8). Because the k = 4 and k = 1 curves are nearly parallel one to another in Fig. 9, the translational motion of the $Xe_2^+Cl^-$ molecule does not change significantly the 4 → 1 transition energy.

4. Cl Atom at an Interstitial Position

At the interstitial position the Cl atom has 6 nearest-neighbor Xe atoms, so that the system is considered as an Xe_6Cl molecule inside the Xe matrix. The Cartesian coordinates of the atoms and the Xe-Cl distances are presented in Table 3 for the minimum energy configuration. The predominant transition is to the lowest ionic state, k = 4, with a transition moment of 3.72 D and transition energy of 3.37 eV. This energy is lower than the

lowest limit of the absorption band obtained in the previous case for the Cl atom inside a cage (Fig. 7).

The energy to place the Cl atom at the minimum energy interstitial position is 0.104 eV, which is lower than the energy for replacing a Xe atom by a Cl atom, found to be equal to 0.156 eV. However, the difference, 0.05 eV, is too small to make the conclusion that the interstitial position is more stable for the Cl atom than the substitutional site. The energy of the interstitial position is sensitive to the diatomic potentials for relatively short distances (Table 2), where the accuracy of the diatomic potential presentation is low.[16]

In the lowest ionic state, k = 4, the $Xe_6^+Cl^-$ geometry is almost symmetrical with a slight shift of 0.007-0.12 Å from the lattice points. The distance from the Cl atom to one of the Xe atoms is 3.16 Å and 3.78 Å to the other Xe atoms. The state k = 4 is purely ionic with approximately uniform delocalization of the positive charge among the six Xe atoms.

The $Xe_6^+Cl^-$ transition energy to the ground state is 2.32 eV, which is close to the center of the experimental emission band (2.16 eV).[1] However, it is difficult to identify the experimental emission as produced by the $Xe_6^+Cl^-$ molecules. The emission band of the $Xe_6^+Cl^-$ molecule, as well as the absorption band of the Cl atom in the interstitial position, is expected to be relatively narrow, which contradicts the experimental data (see below). It is important also to note that the quasistable $Xe_6^+Cl^-$ molecule is a configuration with a local energy minimum, which may relax to the $Xe_2^+Cl^-$ configuration. However, the possibility of such relaxation is not studied here.

5. Experimental Spectra

The emission spectrum of $Xe_2^+Cl^-$ in solid xenon is shown in Fig. 10. The assignment of this spectrum to the molecular triatomic exciplex and its simulation by gas-phase pair potentials was presented in Ref. 1. The emission is centered at 2.16 eV and has a width of 0.22 eV (FWHM). These values are in acceptable agreement with those calculated in the present model, namely a line center of 2.35 eV and a linewidth of 0.2-0.28 eV for the 4 → 1 transition (see Sec. 3).

Excitation spectra of Cl atoms trapped in solid xenon, xenon:argon and xenon:krypton were reported in Ref. 1. The spectra are broad and power dependent. The weak-field excitation spectra are of concern here, which were obtained by monitoring the triatomic emission while scanning the monochromatized output of a xenon-arc lamp. Two such spectra are shown in Fig. 11, where 11a was recorded immediately after photogeneration of the Cl atoms by laser irradiation at 308 nm, while 11b was recorded after annealing the solid at 55 K. The preannealed spectrum shows a single broad peak at 3.5 eV. Upon annealing, the spectrum undergoes a permanent change: several secondary peaks develop in the range 3.5-4.5 eV, and the preannealed peak diminishes to a shoulder near the absorption threshold. Once annealed, the spectrum only undergoes reversible changes in linewidth with thermal cycling. It is worth noting that while a well-defined absorption threshold is observed in these spectra, the short- wavelength limit of 260 nm is strictly experimental.

Permanent change of absorption spectra upon annealing is diagnostic of intersite conversion. Reversible line-broadening with temperature cycling is diagnostic of population equilibrium among thermally accessible initial states. The single-peaked preannealed spectrum is then indicative of a

tight trapping site with little variation in the Cl-Xe nearest-neighbor distances. The broad multiple-peaked spectrum after annealing is indicative of a looser trapping site in which a variety of Cl-Xe distances coexist and are accessible thermally. The likely assignment is then that the preannealed spectrum is due to interstitially trapped Cl, while the annealed spectrum represent substitutionally trapped Cl atoms. The spectra are then in general agreement with calculations, namely that absorption at interstitial sites leads to a single narrow spectral distribution while absorption at substitutional sites leads to a spectral distribution that shows an energy range of ~ 1 eV (compare Figs. 7 and 11). The calculated absorption maxima, 3.37 eV for the interstitial position and ~ 3.65 eV (Fig. 7b) at the substitutional site, are located close to the corresponding experimental values of 3.5 eV and ~ 3.75 eV.

Independent of the exact assignment of the different sites, if different ionic states are favored in the different sites, then the emission spectra would depend on the excitation wavelength, temperature and annealing history of the solid. Emission spectra identical to that shown in Fig. 10 are obtained for excitation wavelengths ranging from 375 to 280 nm, and for temperatures ranging from 12 to 40 K. The result of annealing is a permanent line-narrowing of ~ 200 cm^{-1}. The latter observation is verification of the inhomogeneity of observed lineshapes; yet in all cases the emission lineshapes are indistinguishable. The experiments then clearly establish that independent of the initial isolation site of the dopants, and therefore independent of the initial configuration of the charge-transfer complex accessed optically, the system always relaxes to the lowest energy configuration, namely $Xe_2^+Cl^-$.

6. Conclusions

1. A Cl atom in a substitutional site can move inside the Xe cage almost freely over distances $\lesssim$ 1 Å at the temperatures 10-20 K. The Cl atom is mostly shifted toward the cage Xe atoms.

2. Due to the Cl motion inside the Xe cage, the energy spectrum of the excitation to ionic activated complexes is broadened and has two wide maxima in the regions 320-340 nm and 270-290 nm.

3. The positive charge in the ionic activated complexes is distributed most often between several Xe atoms forming, in general, a $Xe_{12}^{+}Cl^{-}$ molecule.

4. In the lowest ionic state, a quasistable $Xe_2^{+}Cl^{-}$ molecule is formed in the configuration similar to that of the gas-phase $Xe_2^{+}Cl^{-}$ molecule. The calculated decrease of the emission photon energy by the matrix is 0.21 eV, in comparison with ~0.36 eV in the experiment. The inner vibrational motion of the $Xe_2^{+}Cl^{-}$ molecule increases the width of the emission band to 0.3 eV, approximately.

5. In the interstitial position of the Cl atom the quasistable $Xe_6^{+}Cl^{-}$ ionic molecule can be formed. The calculated emission frequency of this molecule is close to the experimental value; however the emission band can not be as wide as in the experiment. It follows that most probably not the $Xe_6^{+}Cl^{-}$ but the $Xe_2^{+}Cl^{-}$ molecule, formed in the substitutional site, is responsible for the experimentally detected emission.

Acknowledgments

This research was supported by the National Science Foundation under Grant CHE-8620274, the Air Force Office of Scientific Research (AFSC), United State Air Force, under Contract F49620-86-C-0009, and the Office of Naval Research. The United State Government is authorized to reproduce and distribute reprints for governmental purpose notwithstanding any copyright

notation hereon. I. L. thanks SUNY-Buffalo for its hospitality during a visit in 1986-87 when this work was performed.

References

1. M. E. Fajardo and V. A. Apkarian, J. Chem. Phys. 85, 5660 (1986).
2. M. E. Fajardo and V. A. Apkarian, Chem. Phys. Lett. 134, (1987).
3. B. S. Ault and L. Andrews, J. Chem. Phys. 65, 4192 (1976).
4. J. Goodman and L. E. Brus, J. Chem. Phys. 65 3808 (1976).
5. J. Le Calvé and M. Chergui, Chem. Phys. Lett. 132, 156 (1986).

6(a). V. S. Dubov, L. I. Gudzenko, L. V. Gurvich and S. I. Iakovlenko, Chem. Phys. Lett. 53, 170 (1978); (b) V. S. Dubov, Y. E. Lapsker, A. N. Samoilova and L. V. Gurvich, Chem. Phys. Lett. 83, 518 (1981).

7. H. P. Grieneisen, H. Xue-Jing and K. L. Kompa, Chem. Phys. Lett. 82, 421 (1981).
8. B. E. Wilcomb and R. Burnham, J. Chem. Phys. 74, 6784 (1981).

9(a). A. W. McCown and J. C. Eden, J. Chem. Phys. 81, 1933 (1984).(b) A. W. McCown, M. N. Ediger, D. B. Geohegan and J. G. Eden, J. Chem. Phys. 82, 4862 (1985).

10(a). G. Inoue, J. K. Ku and D. W. Setser, J. Chem. Phys. 76, 733 (1982); (b) ibid., 80, 6006 (1984); (c) Y. C. Yu, D. W. Setser and H. Horiguchi, J. Phys. Chem. 87, 2209 (1983); (d) D. W. Setser and J. Ku, in Photophysics and Photochemistry above 6 eV, ed. by F. Lahmani (Elsevier, New York, 1985), p. 621 ff.

11. M. Boivineau, J. Le Calvé, M. C. Castex and C. Jouvet, Chem. Phys. Lett. 128, 528 (1986); J. Chem. Phys. 84, 4712 (1986).
12. H. Jara, J. Pummer, H. Egger and C. K. Rhodes, Phys. Rev. B 30, 1 (1984).
13. L. Wiedeman, M. E. Fajardo and V. A. Apkarian, Chem. Phys. Lett. 134, 55 (1987).

14. I. Last and T. F. George, J. Chem. Phys. 86, 3787 (1987).

15. D. L. Andrews and M. J. Harlow, J. Chem. Phys. 78, 1088 (1983); 80, 4753 (1984).

16. I. Last and T. F. George, J. Chem. Phys. (in press).

17. W. J. Stevens and M. Krauss, Appl. Phys. Lett. 47, 301 (1984).

18. D. L. Huestis, G. Marowsky and F. K. Tittel, in Excimer Lasers - 1983, ed. by C. K. Rhodes, H. Egger and H. Pummer (American Institute of Physics, New York, 1983), pp. 238-248.

Table 1. Angular and Cartesian coordinates of the cage Xe atoms, R = 3.062 Å

\ i	1	2	3	4	5	6	7	8	9	10	11	12
θ	90	45	45	90	45	45	90	135	135	90	135	135
ϕ	45	0	90	135	180	270	315	0	90	225	180	270
x	R	R	0	-R	-R	0	R	R	0	-R	-R	0
y	R	0	R	R	0	-R	-R	0	R	-R	0	-R
z	0	R	R	0	R	R	0	-R	-R	0	-R	-R

Table 2. Cartesian coordinates (in Å) of atoms for the $Xe_2^+Cl^-$ equilibrium configuration. The coordinates of the i = 4-12 Xe atoms are the same as in Table 1.

		Xe		
	Cl \ i	1	2	3
x	1.114	2.887	2.887	0
y	-0.083	2.670	0.329	3.132
z	0.038	0.329	2.670	3.132
R_{XeCl}	-	3.30	3.30	4.68

Table 3. Cartesian coordinates (in Å) of the Cl atom at an interstitial position and six neighboring Xe atoms for the ground state.

		Xe					
	Cl \ i	1	2	3	4	5	6
x	0	0	0	3.48	-3.48	0	0
y	0	0	0	0	0	3.48	-3.48
z	-0.65	-3.46	2.76	0	0	0	0
R_{Xe-Cl}	-	2.81	3.41	3.54	3.54	3.54	3.54

Figure Captions

Fig. 1. Angular Coordinates and the location the three Xe atoms (i = 1,2,3) of the cage.

Fig. 2. Ground state potential energy surfaces of the Cl atom in the Xe cage for the planes passing through the z-axis (the ordinate). The numbers next to the equipotential lines indicate their energy in eV. The pointers indicate the direction to the nearest Xe atom. The planes for the following values of the angle coordinates ϕ are presented: a) $\phi = 0^\circ$, b) $\phi = 15^\circ$, c) $\phi = 30^\circ$, d) $\phi = 45^\circ$. For the location of the planes relatively to the Xe atoms see Table 1.

Fig. 3. Average distance $\bar{R}$ of the Cl atom from the cage center (the left scale) and light absorption cross section Q (the right scale) as functions of temperature.

Fig. 4. Potential curves of all ionic states (k = 4-39) along the line running from the cage center to the nearest Xe atom. The distance of the Cl atom from the cage center is plotted against the x-axis.

Fig. 5. Potential curves of the lowest ionic states k = 4-15 along arcs with a fixed radius R = 1.1 Å. The angle shift of the Cl atom on an arc is plotted against the x-axis.

(a) The arc is located in a plane which includes the cage center and two Xe atoms. The curves start at the point on the line running to one of these atoms and end at the point on the line running between these two Xe atoms.

(b) The arc is located in the $\theta = 90^\circ$ (the xy-plane). The curves start at the point on the x-axis ($\phi = 0^\circ$) which is equidistant to

four Xe atoms and end at the point on the line running to one of these atoms ($\phi = 45°$).

Fig. 6. Potential energy surfaces of the Cl^- ion in the Xe_{12}^+ cage for the lowest ionic states k = 4 (a) and k = 5 (b) in the plane $\phi = 0°$ which is the same as in Fig. 1a for the ground state. The numbers next to the equipotential lines show their energy in eV.

Fig. 7. The energy spectrum of the excitation of the $Xe_{12}Cl$ system from neutral (k = 1-3) to ionic (k = 4-39) states (see the text). The solid line represents the total excitation. The dashed lines represent the excitations to the particular ionic states k = 4,5,20. The spectrum is given for the temperatures 10 K (a) and 80 K (b).

Fig. 8. The Xe_2Cl potential curves of the first ionic state k = 4 (the left scale) and the ground state k = 1 (the right scale) in the vicinity of the $Xe_2^+Cl^-$ (k = 4) equilibrium configuration (Table 2) for the fixed molecular plane and fixed Cl atom location:

(a) Potential curves as functions of the Xe-Cl molecular distance.

(b) Potential curves as functions of the Xe-Cl-Xe molecular angle.

Fig. 9. Xe_2Cl potential curves of the first ionic state k = 4 (the left scale) and the ground state k = 1 (the right scale) in the $Xe_2^+Cl^-$ (k = 4) equilibrium configuration as functions of the molecule translation shift along following mutually perpendicular lines:

(a) x-axis ($\theta = 90°$, $\phi = 0°$).

(b) The (+yz) diagonal line ($\theta = 45°$, $\phi = 90°$)

(c) The (-yz) diagonal line ($\theta = 45°$, $\phi = 270°$)

The lines (a) and (b) lie in the system symmetry plane which is perpendicular to the molecular plane; the line (c) lies in the molecular plane.

Fig. 10. Emission spectrum of $Xe_2^+Cl^-$ in solid xenon at 12 K. Original composition, 1:100 HCl:Xe; excitation wavelength, 308 nm.

Fig. 11. Excitation spectra of Cl:Xe solids at 12 K. Original composition, 1:100 HCl:Xe. The spectra were recorded with weak-field excitation after extensive irradiation of the solid with a 308 nm laser: (a) spectrum recorded prior to annealing the solid; (b) spectrum recorded after extensive annealing at 55 K.

Fig. 1

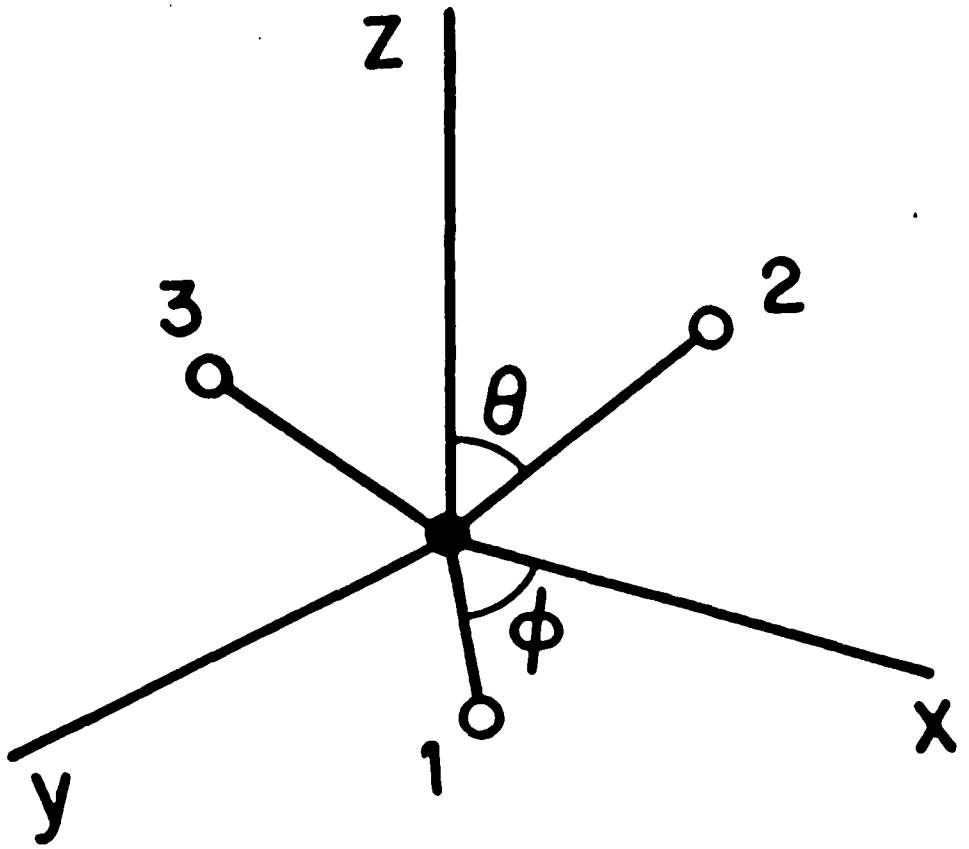

Fig. 2(a)

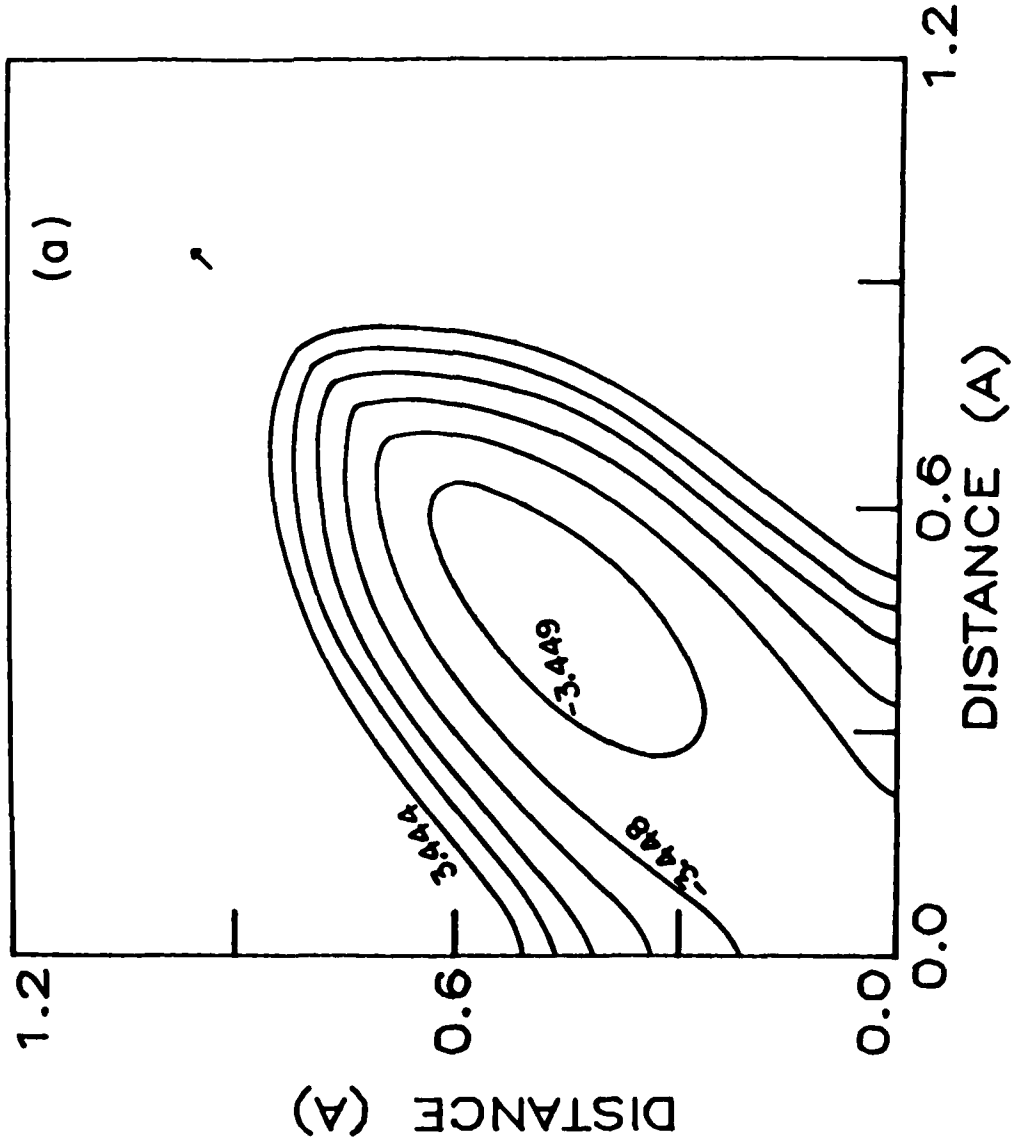

Fig. 2(b)

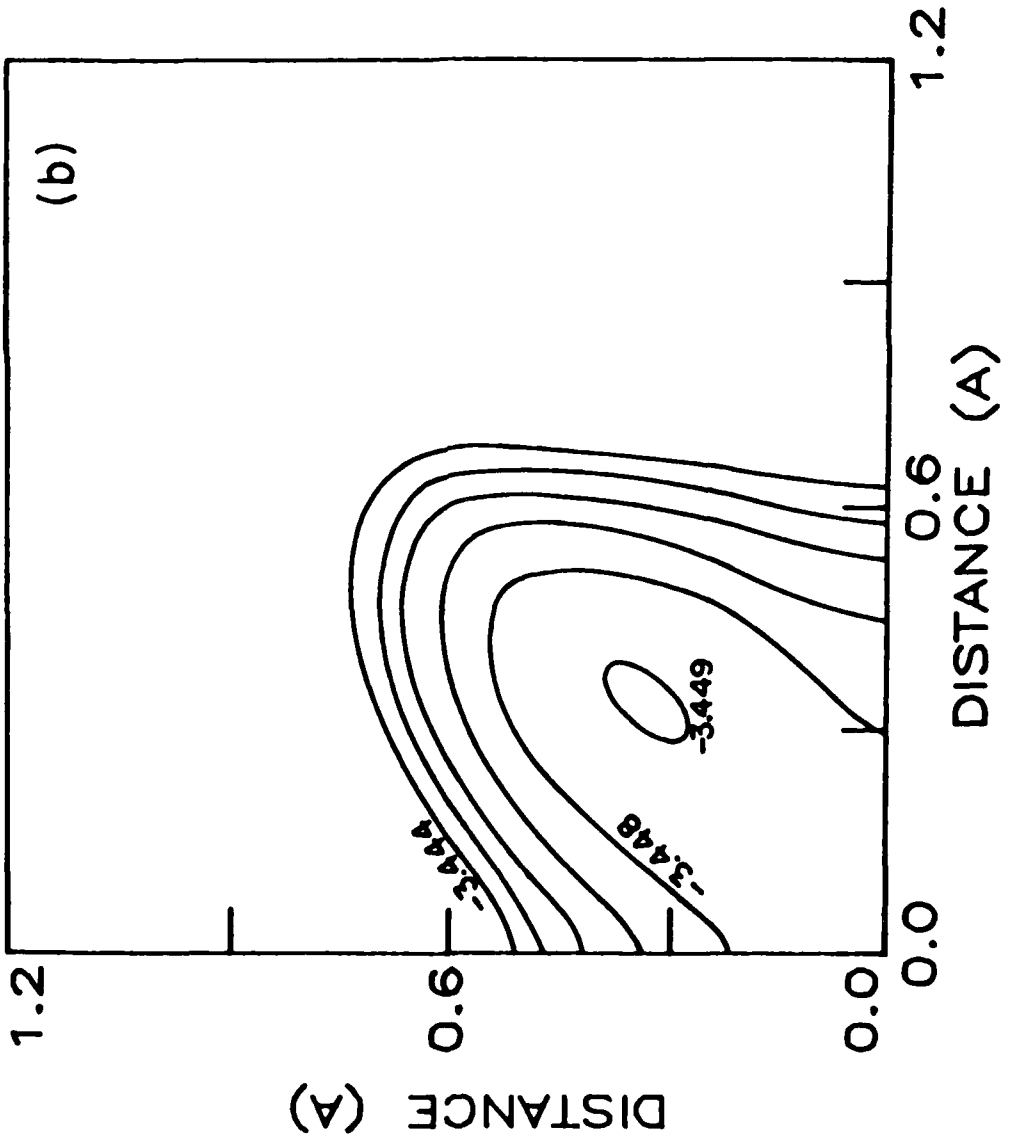

Fig. 2(c)

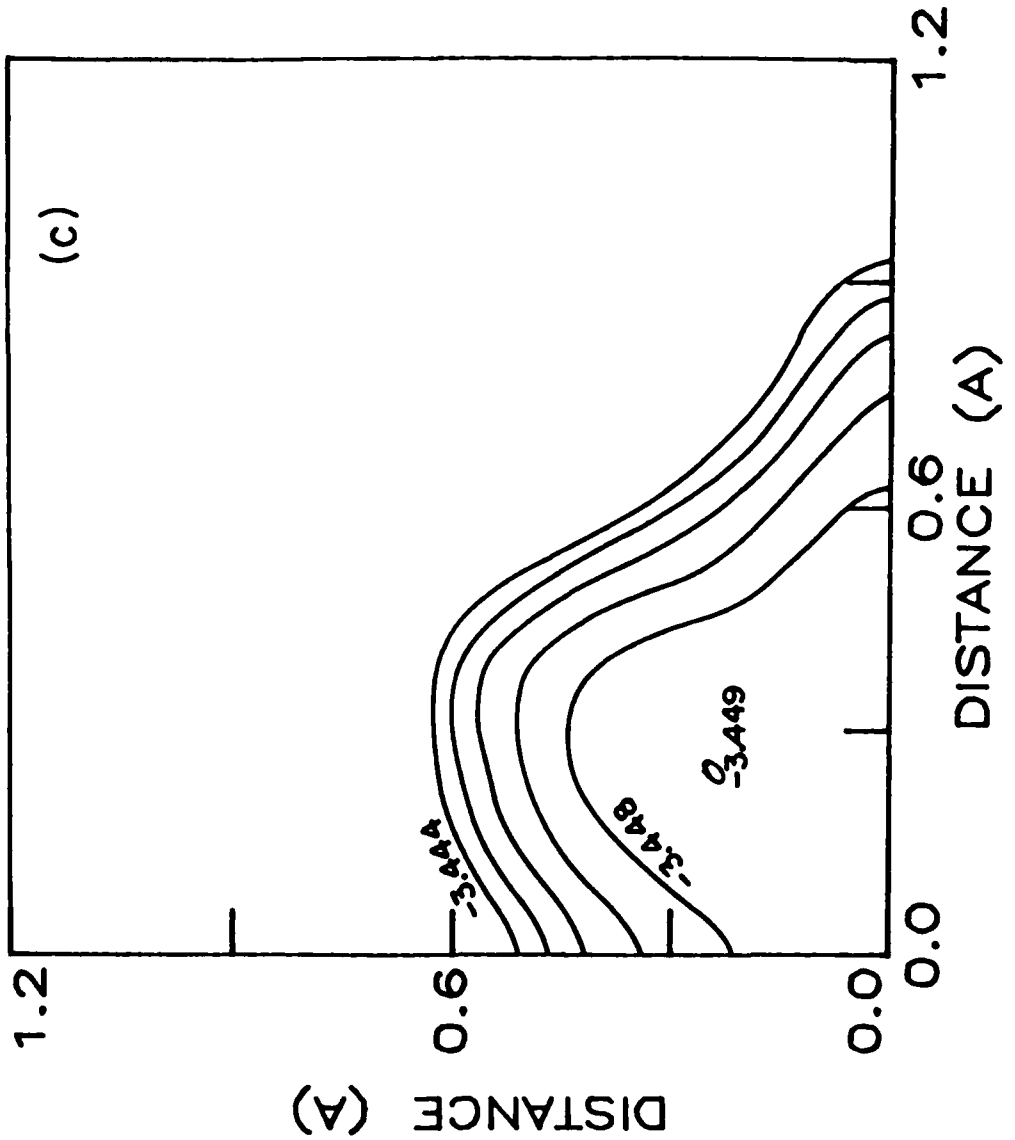

Fig. 2(d)

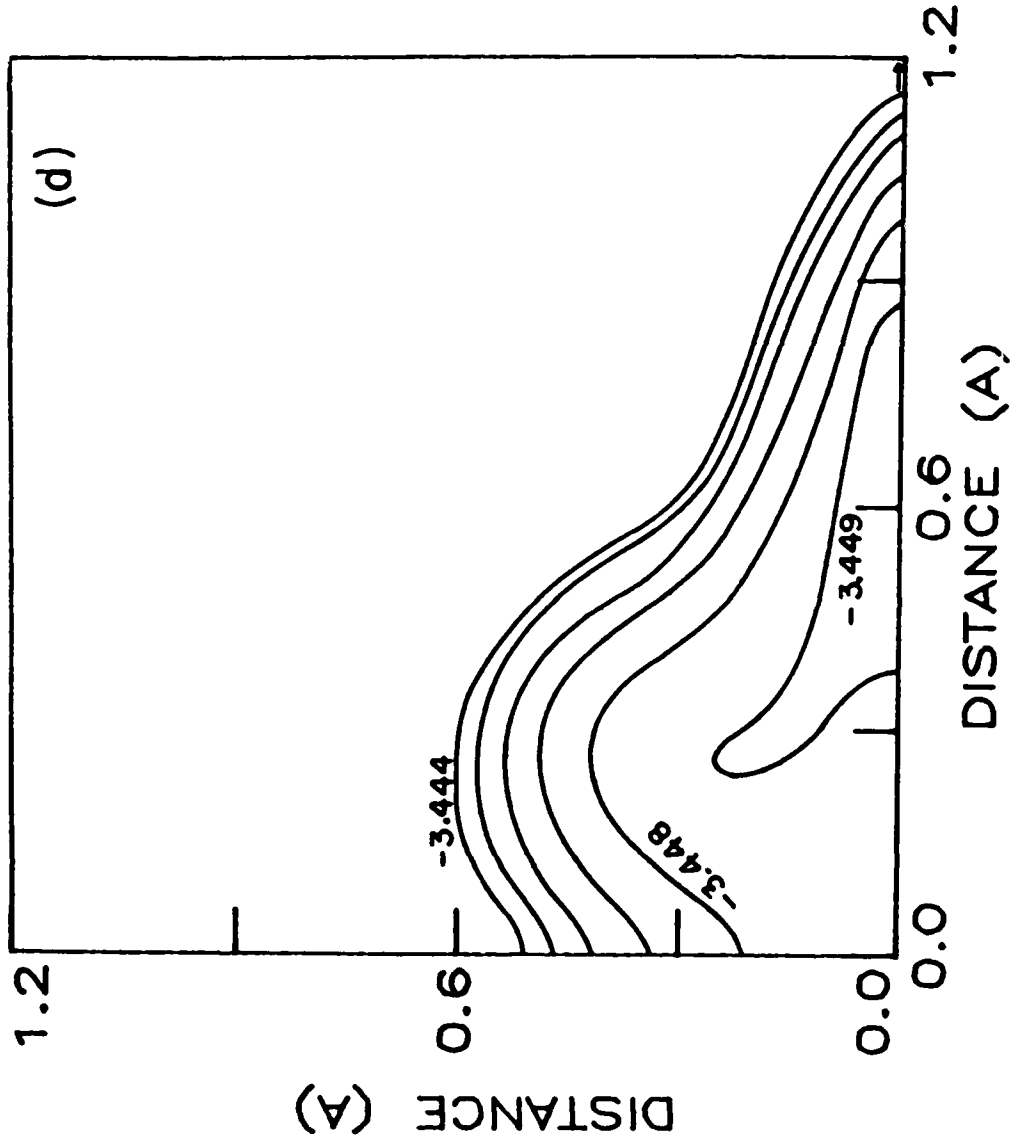

Fig. 3

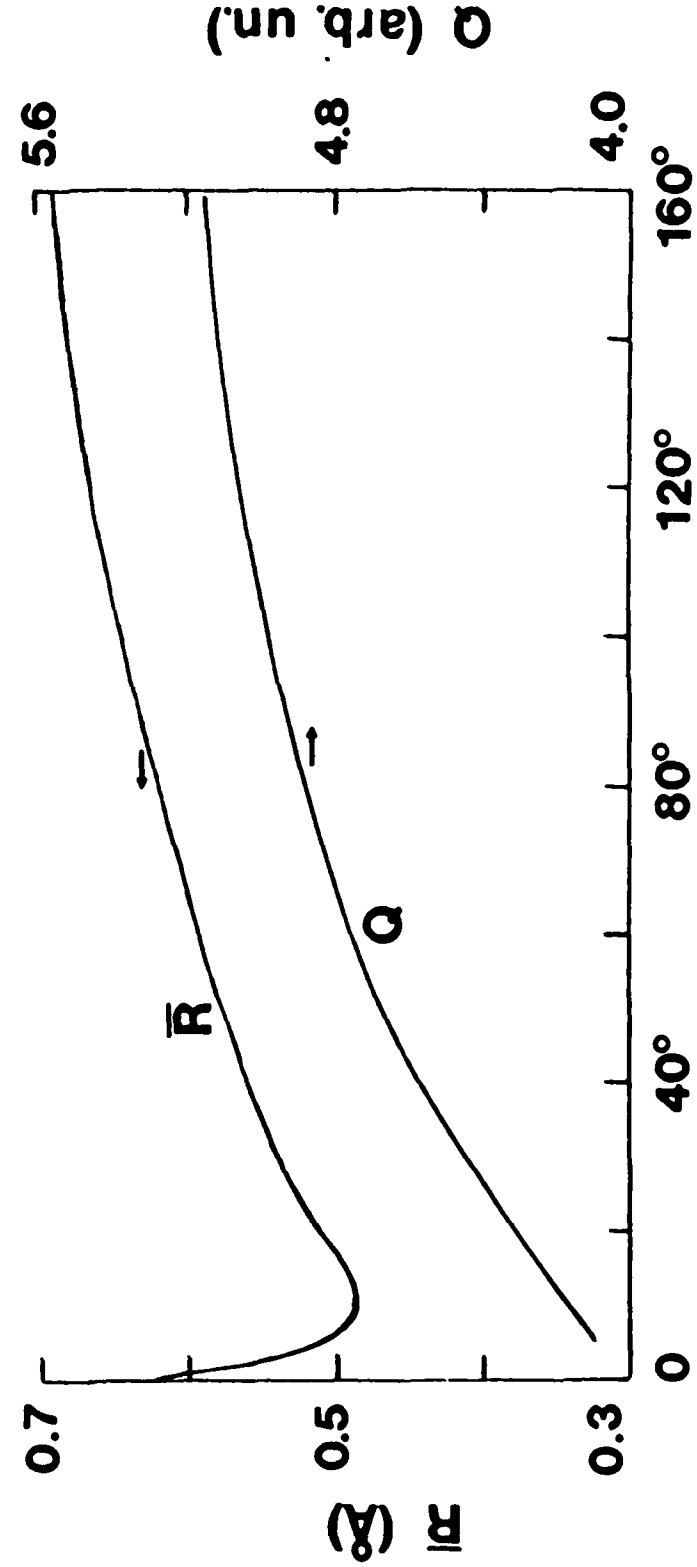

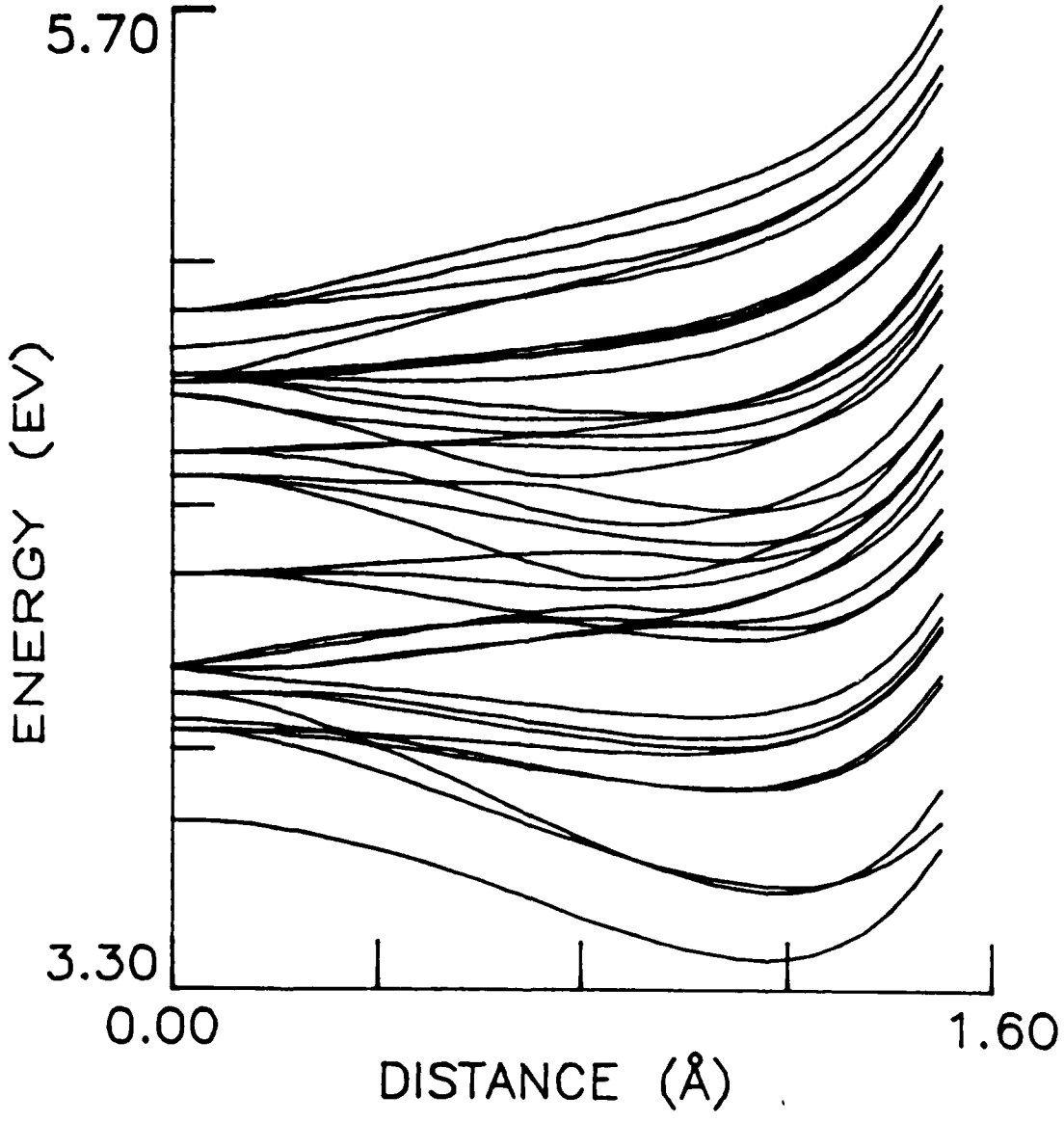

Fig 4

Fig. 5(a)

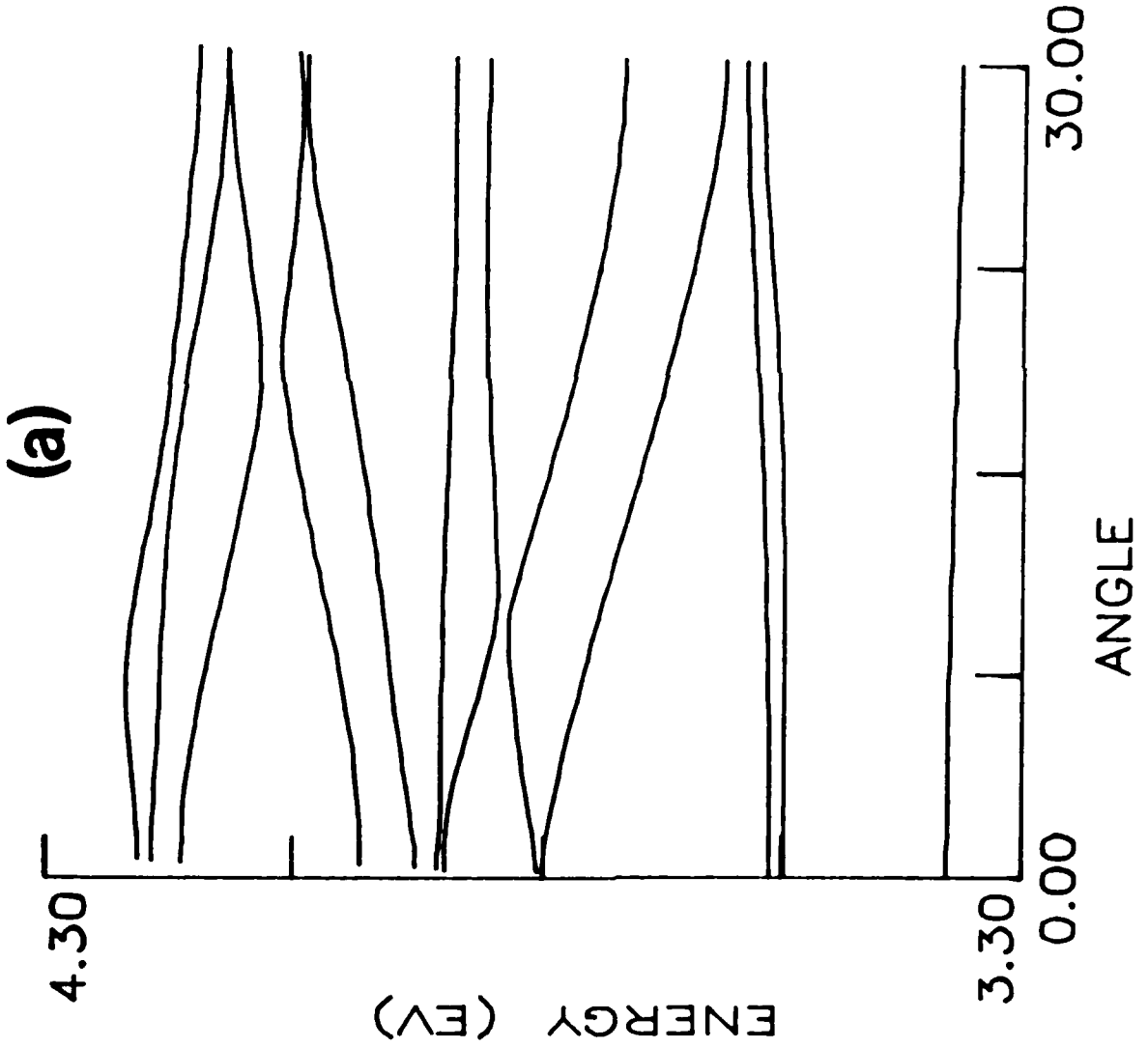

Fig. 5 (b)

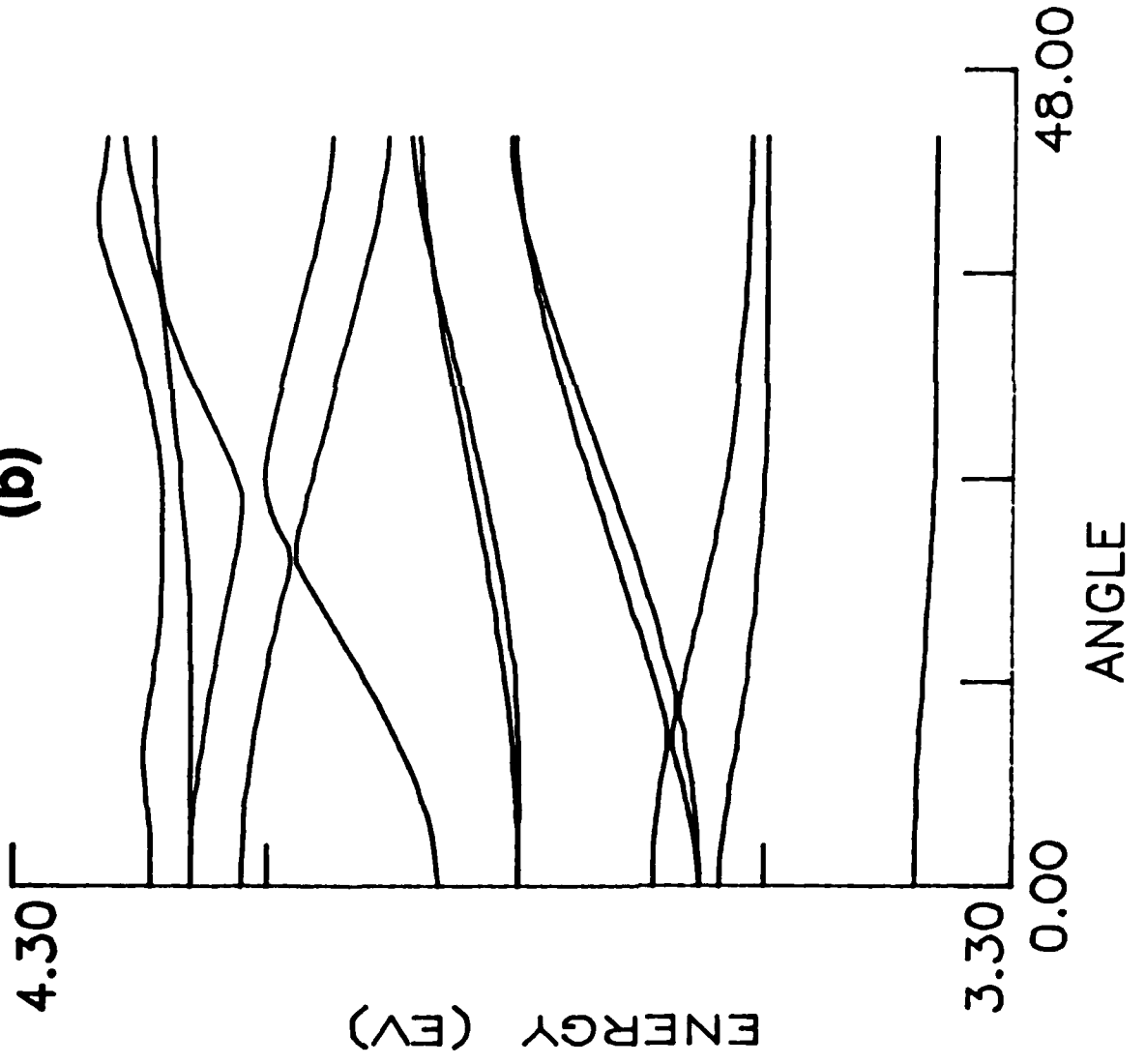

Fig 6(a)

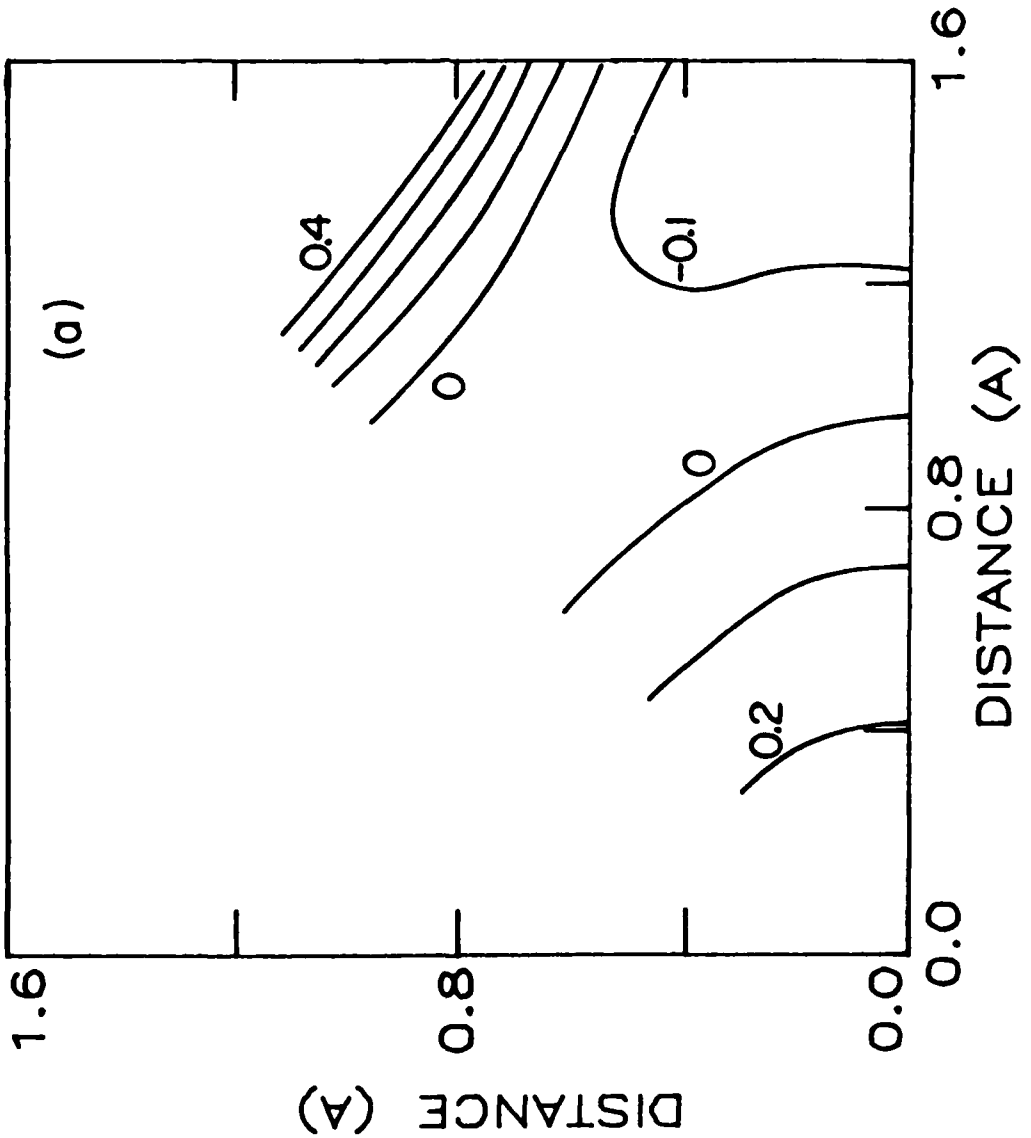

Fig 6(b)

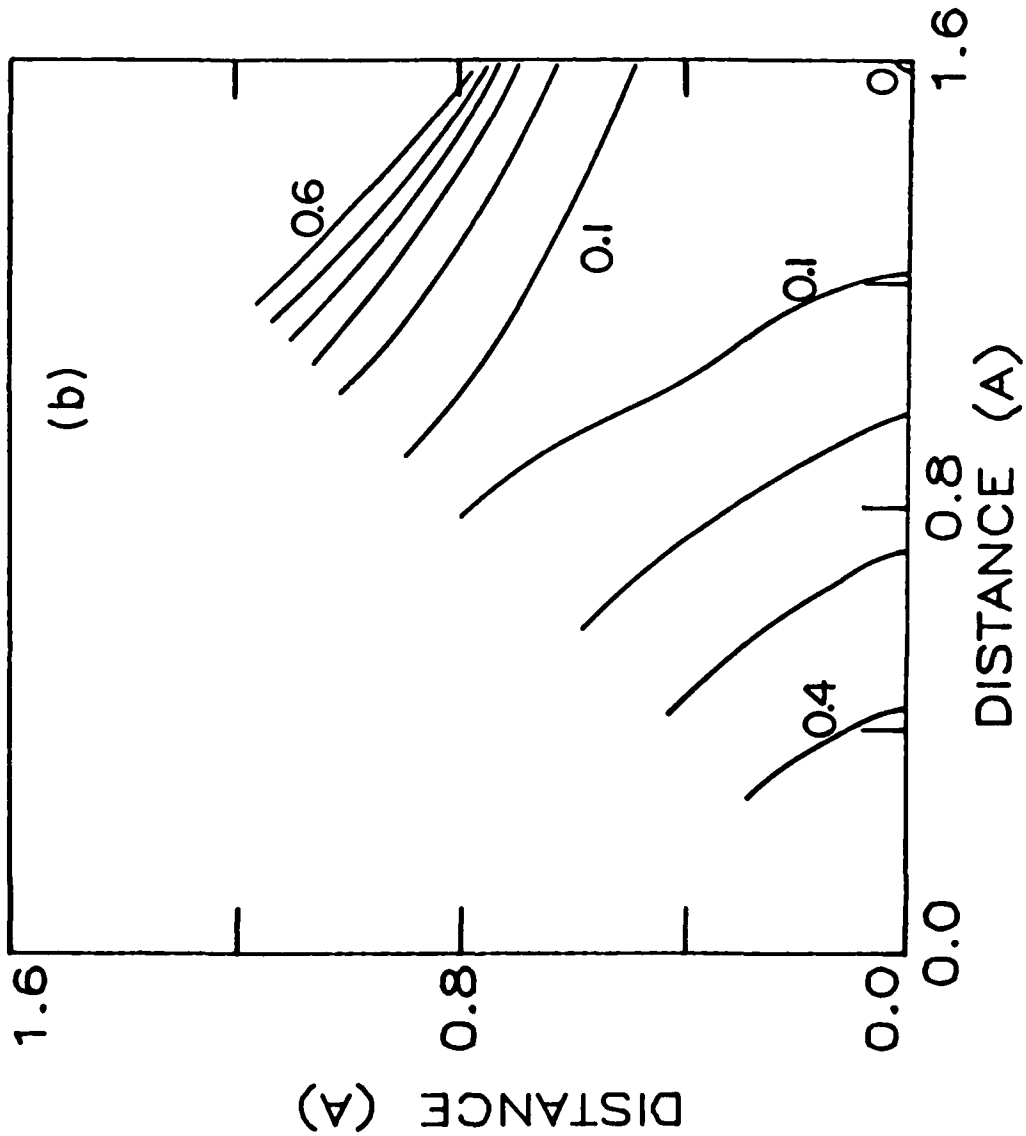

Fig. 7(a)

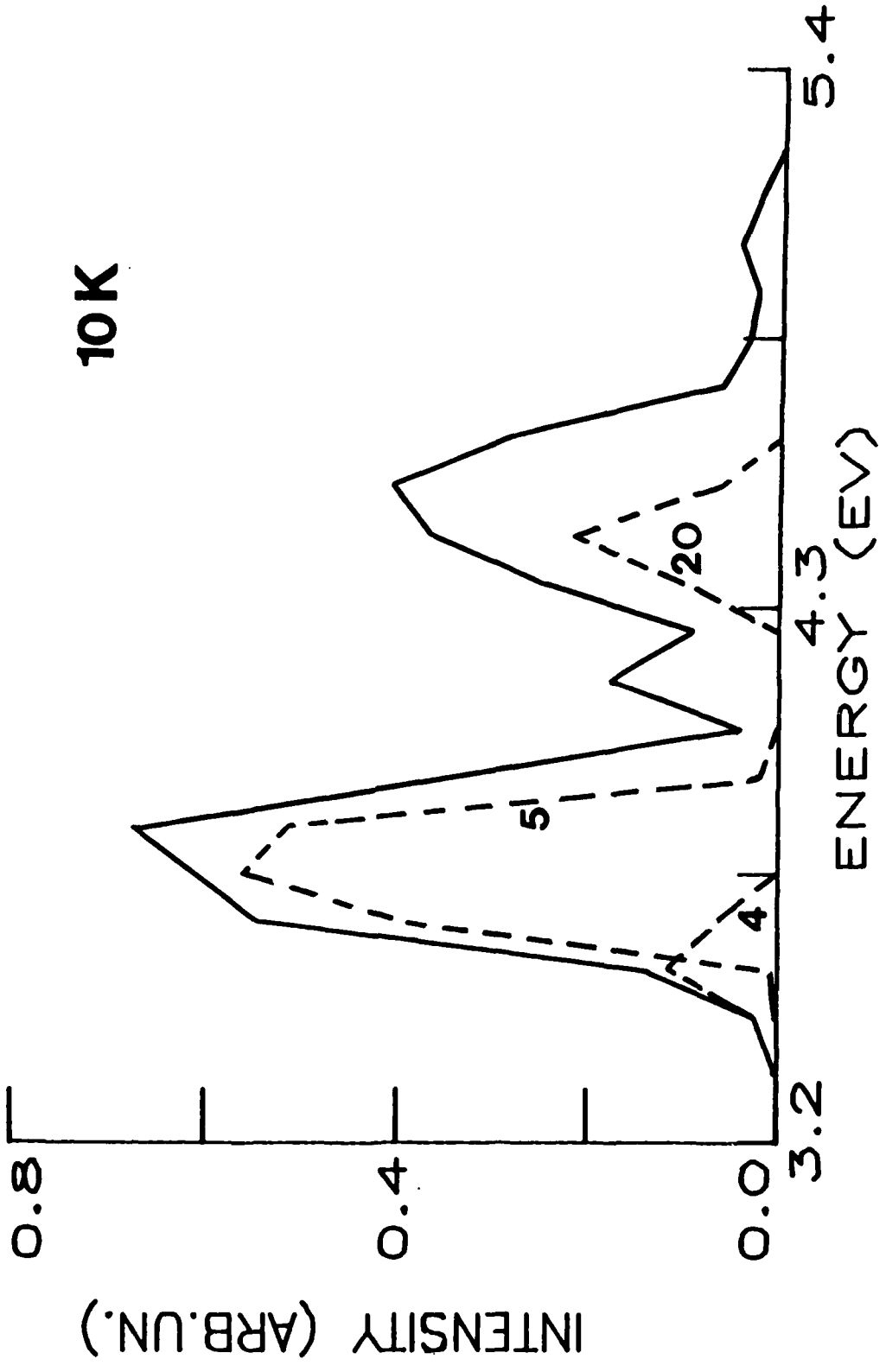

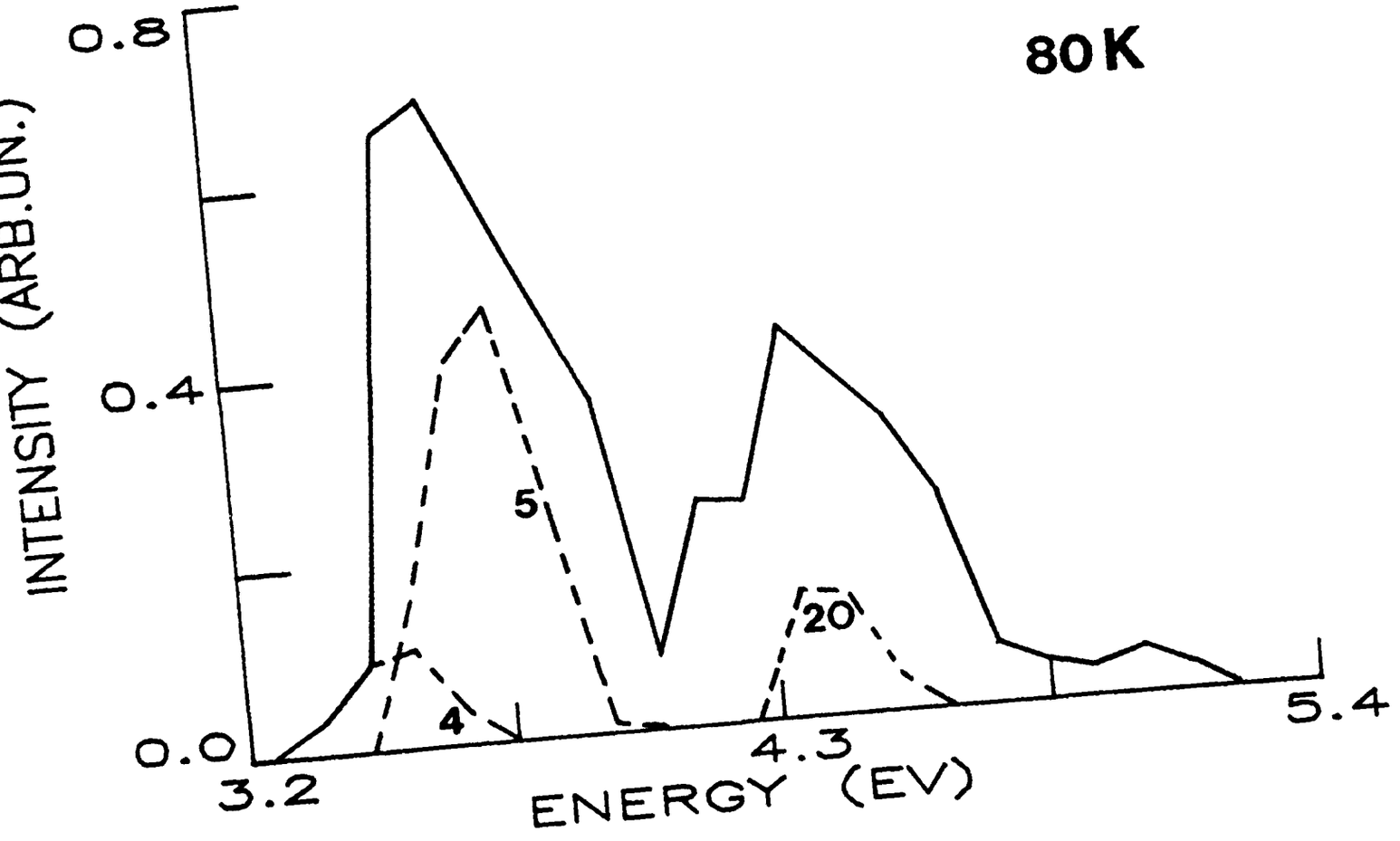

Fig. 7(a)

Fig 8 (a)

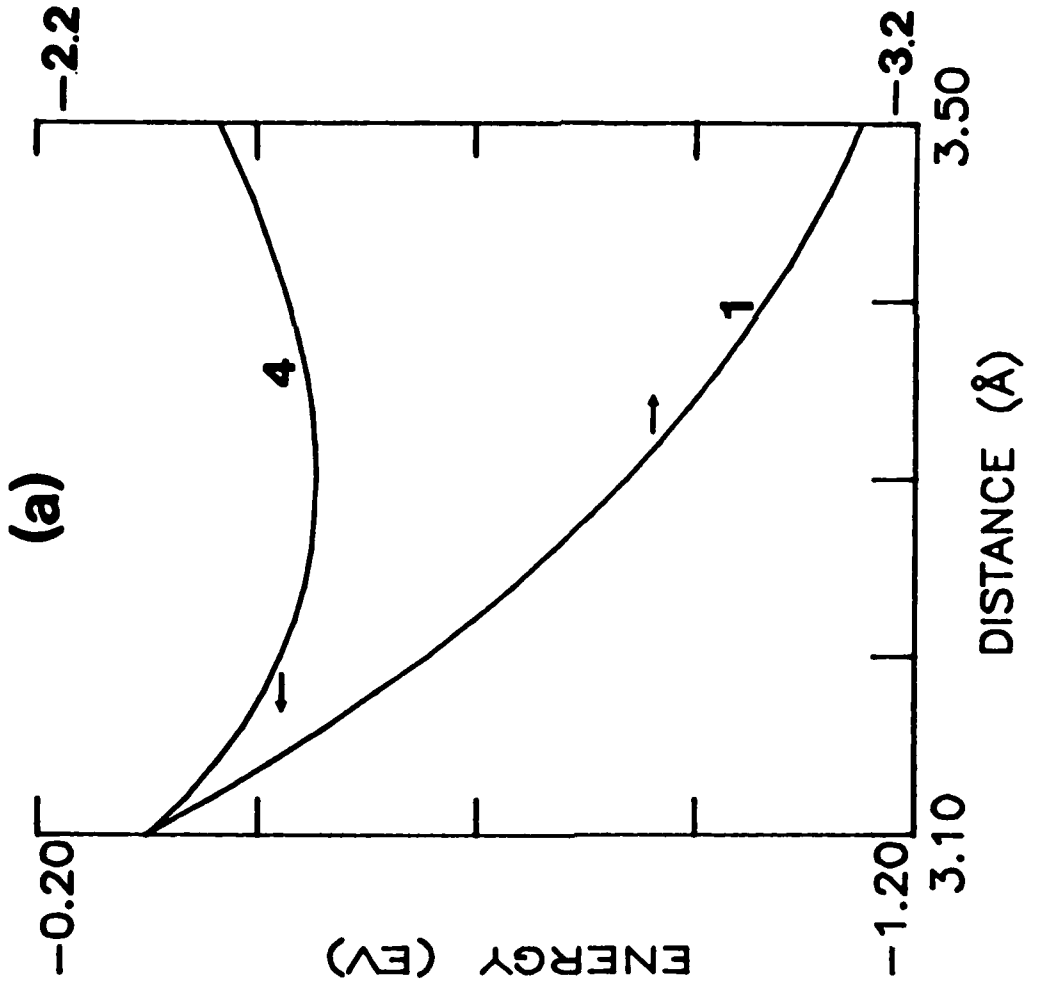

Fig. 8 (b)

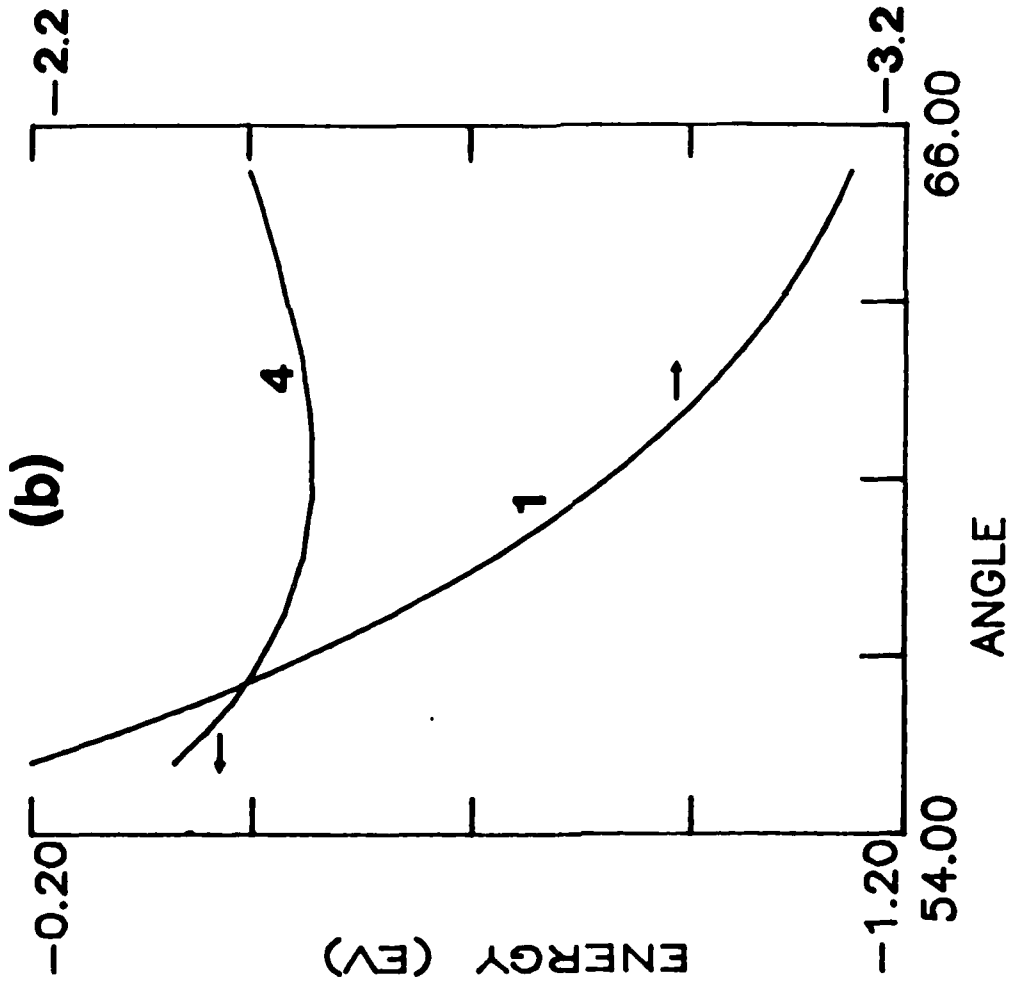

Fig. 9(a)

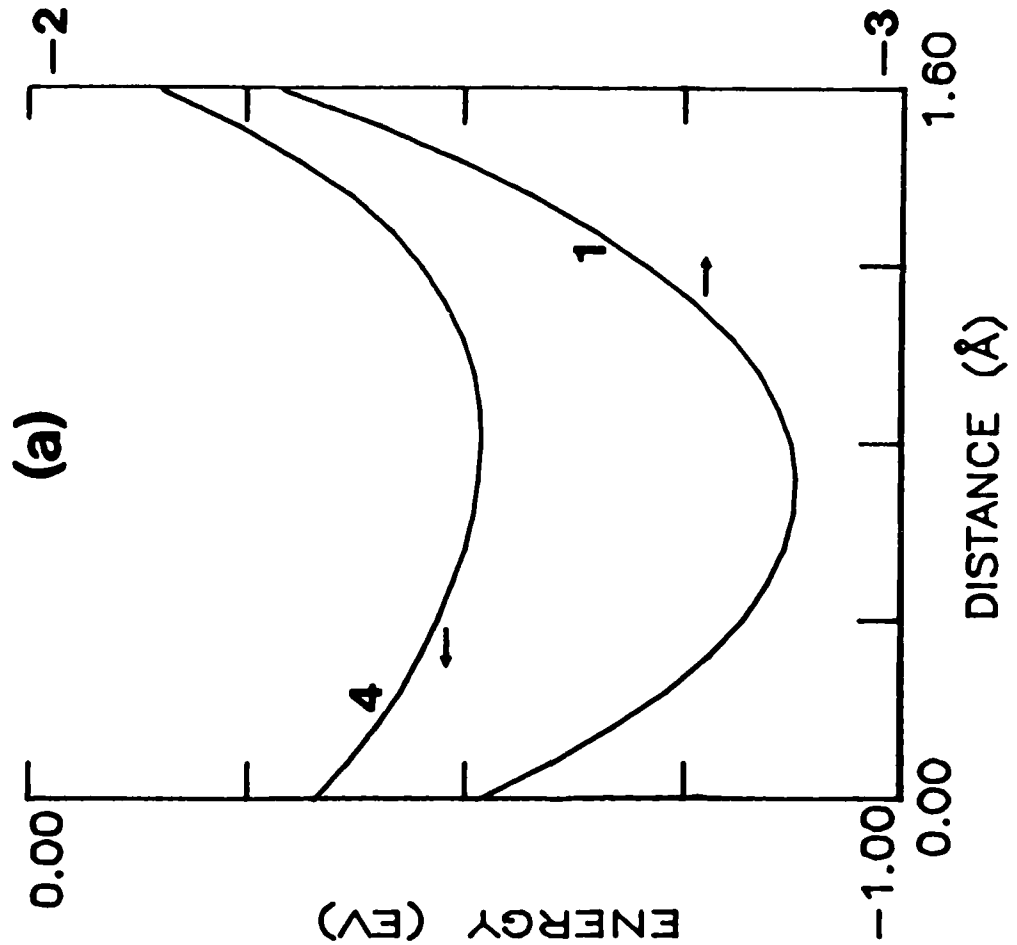

Fig. 9(b)

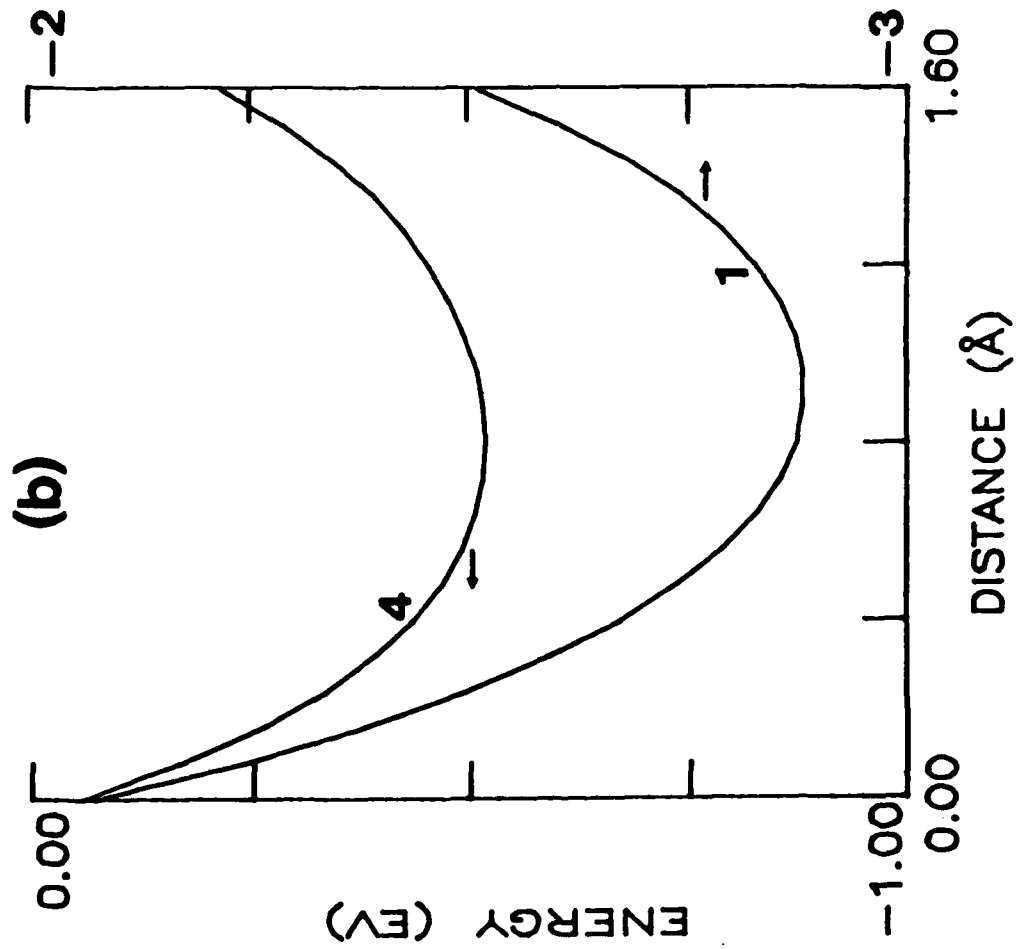

Fig. 9(c)

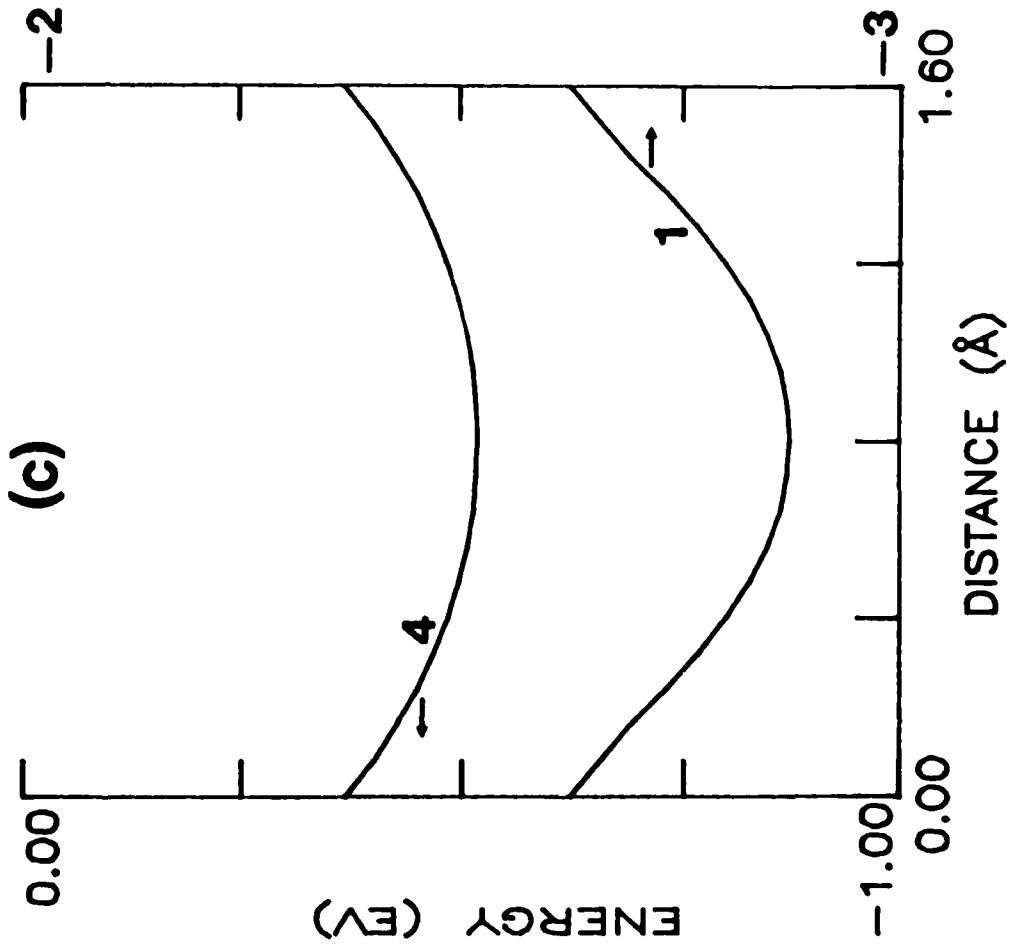

Fig. 10

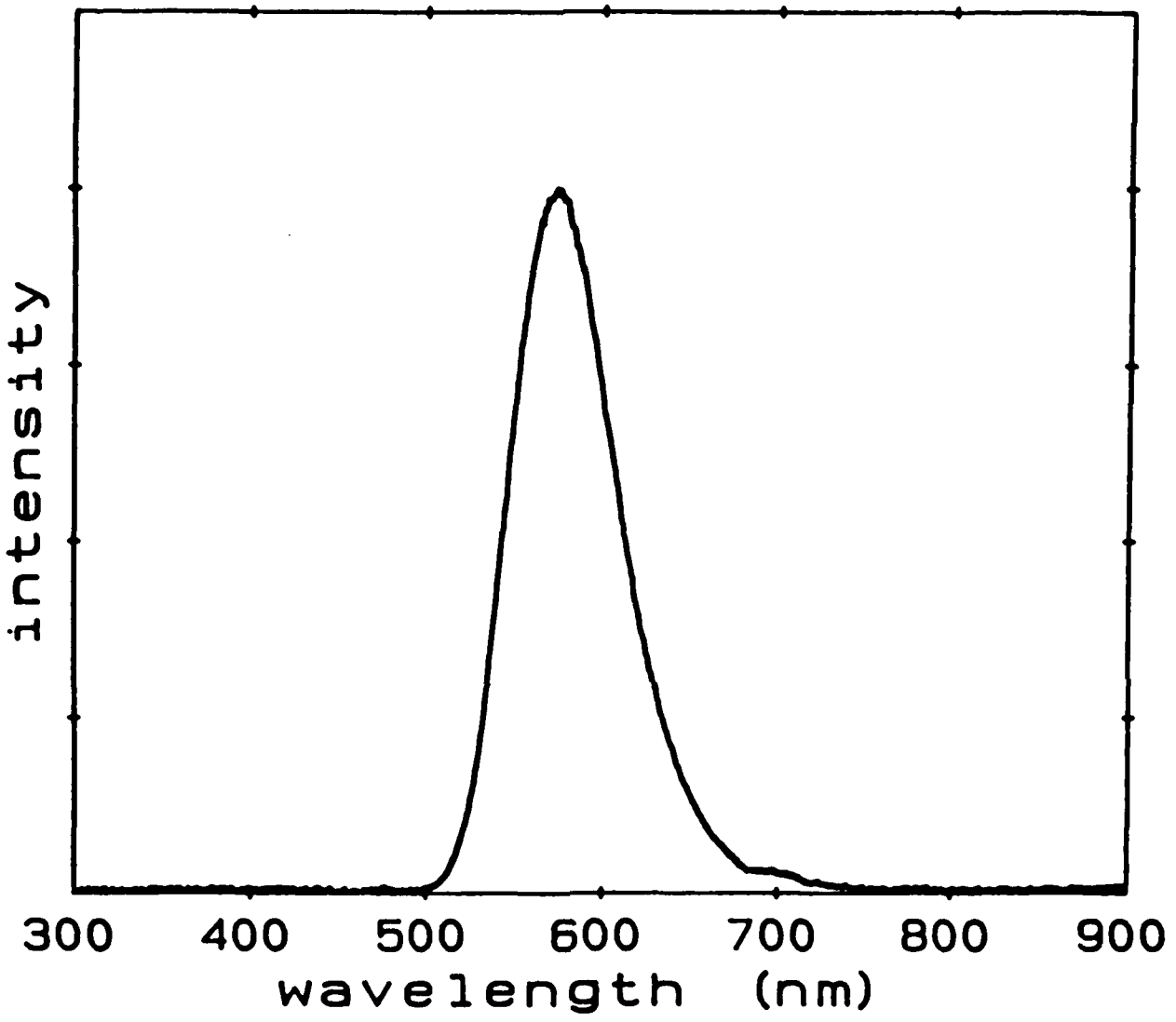

Fig. 11

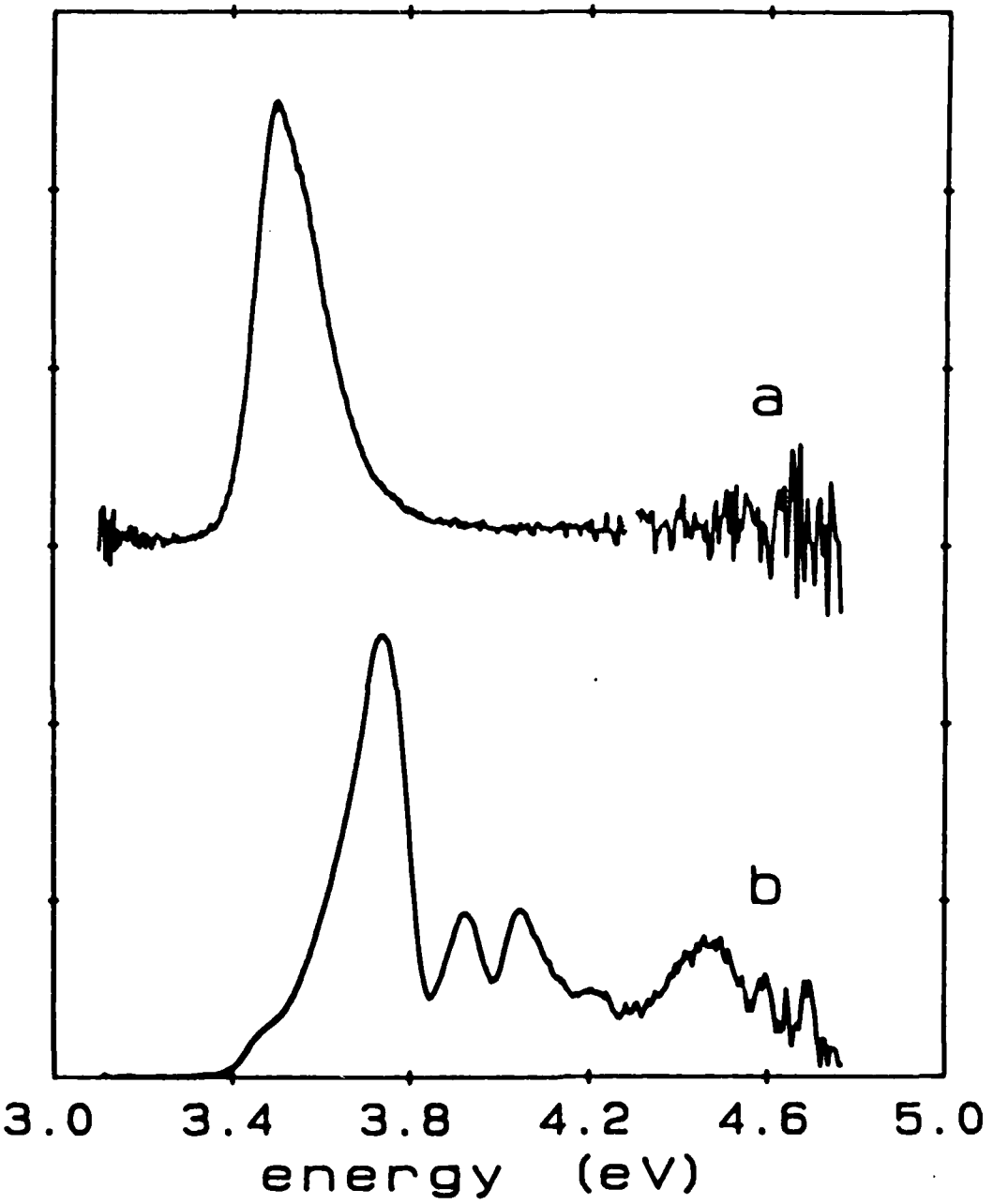

TECHNICAL REPORT DISTRIBUTION LIST, GEN

	No. Copies
Office of Naval Research Attn: Code 1113 800 N. Quincy Street Arlington, Virginia 22217-5000	2
Dr. Bernard Douda Naval Weapons Support Center Code 50C Crane, Indiana 47522-5050	1
Naval Civil Engineering Laboratory Attn: Dr. R. W. Drisko, Code L52 Port Hueneme, California 93401	1
Defense Technical Information Center Building 5, Cameron Station Alexandria, Virginia 22314	12 high quality
DTNSRDC Attn: Dr. H. Singerman Applied Chemistry Division Annapolis, Maryland 21401	1
Dr. William Tolles Superintendent Chemistry Division, Code 6100 Naval Research Laboratory Washington, D.C. 20375-5000	1
Dr. David Young Code 334 NORDA NSTL, Mississippi 39529	1
Naval Weapons Center Attn: Dr. Ron Atkins Chemistry Division China Lake, California 93555	1
Scientific Advisor Commandant of the Marine Corps Code RD-1 Washington, D.C. 20380	1
U.S. Army Research Office Attn: CRD-AA-IP P.O. Box 12211 Research Triangle Park, NC 27709	1
Mr. John Boyle Materials Branch Naval Ship Engineering Center Philadelphia, Pennsylvania 19112	1
Naval Ocean Systems Center Attn: Dr. S. Yamamoto Marine Sciences Division San Diego, California 91232	1
Dr. David L. Nelson Chemistry Division Office of Naval Research 800 North Quincy Street Arlington, Virginia 22217	1

ABSTRACTS DISTRIBUTION LIST, 056/625/629

Dr. J. E. Jensen
Hughes Research Laboratory
3011 Malibu Canyon Road
Malibu, California 90265

Dr. J. H. Weaver
Department of Chemical Engineering
and Materials Science
University of Minnesota
Minneapolis, Minnesota 55455

Dr. A. Reisman
Microelectronics Center of North Carolina
Research Triangle Park, North Carolina
27709

Dr. M. Grunze
Laboratory for Surface Science and
Technology
University of Maine
Orono, Maine 04469

Dr. J. Butler
Naval Research Laboratory
Code 6115
Washington D.C. 20375-5000

Dr. L. Interante
Chemistry Department
Rensselaer Polytechnic Institute
Troy, New York 12181

Dr. Irvin Heard
Chemistry and Physics Department
Lincoln University
Lincoln University, Pennsylvania 19352

Dr. K.J. Klaubunde
Department of Chemistry
Kansas State University
Manhattan, Kansas 66506

Dr. C. B. Harris
Department of Chemistry
University of California
Berkeley, California 94720

Dr. F. Kutzler
Department of Chemistry
Box 5055
Tennessee Technological University
Cookesville, Tennessee 38501

Dr. D. DiLella
Chemistry Department
George Washington University
Washington D.C. 20052

Dr. R. Reeves
Chemistry Department
Renssaeler Polytechnic Institute
Troy, New York 12181

Dr. Steven M. George
Stanford University
Department of Chemistry
Stanford, CA 94305

Dr. Mark Johnson
Yale University
Department of Chemistry
New Haven, CT 06511-8118

Dr. W. Knauer
Hughes Research Laboratory
3011 Malibu Canyon Road
Malibu, California 90265

ABSTRACTS DISTRIBUTION LIST, 056/625/629

Dr. G. A. Somorjai
Department of Chemistry
University of California
Berkeley, California 94720

Dr. J. Murday
Naval Research Laboratory
Code 6170
Washington, D.C. 20375-5000

Dr. J. B. Hudson
Materials Division
Rensselaer Polytechnic Institute
Troy, New York 12181

Dr. Theodore E. Madey
Surface Chemistry Section
Department of Commerce
National Bureau of Standards
Washington, D.C. 20234

Dr. J. E. Demuth
IBM Corporation
Thomas J. Watson Research Center
P.O. Box 218
Yorktown Heights, New York 10598

Dr. M. G. Lagally
Department of Metallurgical
and Mining Engineering
University of Wisconsin
Madison, Wisconsin 53706

Dr. R. P. Van Duyne
Chemistry Department
Northwestern University
Evanston, Illinois 60637

Dr. J. M. White
Department of Chemistry
University of Texas
Austin, Texas 78712

Dr. D. E. Harrison
Department of Physics
Naval Postgraduate School
Monterey, California 93940

Dr. R. L. Park
Director, Center of Materials
Research
University of Maryland
College Park, Maryland 20742

Dr. W. T. Peria
Electrical Engineering Department
University of Minnesota
Minneapolis, Minnesota 55455

Dr. Keith H. Johnson
Department of Metallurgy and
Materials Science
Massachusetts Institute of Technology
Cambridge, Massachusetts 02139

Dr. S. Sibener
Department of Chemistry
James Franck Institute
5640 Ellis Avenue
Chicago, Illinois 60637

Dr. Arnold Green
Quantum Surface Dynamics Branch
Code 3817
Naval Weapons Center
China Lake, California 93555

Dr. A. Wold
Department of Chemistry
Brown University
Providence, Rhode Island 02912

Dr. S. L. Bernasek
Department of Chemistry
Princeton University
Princeton, New Jersey 08544

Dr. W. Kohn
Department of Physics
University of California, San Diego
La Jolla, California 92037

ABSTRACTS DISTRIBUTION LIST, 056/625/629

Dr. F. Carter
Code 6170
Naval Research Laboratory
Washington, D.C. 20375-5000

Dr. Richard Colton
Code 6170
Naval Research Laboratory
Washington, D.C. 20375-5000

Dr. Dan Pierce
National Bureau of Standards
Optical Physics Division
Washington, D.C. 20234

Dr. R. Stanley Williams
Department of Chemistry
University of California
Los Angeles, California 90024

Dr. R. P. Messmer
Materials Characterization Lab.
General Electric Company
Schenectady, New York 22217

Dr. Robert Gomer
Department of Chemistry
James Franck Institute
5640 Ellis Avenue
Chicago, Illinois 60637

Dr. Ronald Lee
R301
Naval Surface Weapons Center
White Oak
Silver Spring, Maryland 20910

Dr. Paul Schoen
Code 6190
Naval Research Laboratory
Washington, D.C. 20375-5000

Dr. John T. Yates
Department of Chemistry
University of Pittsburgh
Pittsburgh, Pennsylvania 15260

Dr. Richard Greene
Code 5230
Naval Research Laboratory
Washington, D.C. 20375-5000

Dr. L. Kesmodel
Department of Physics
Indiana University
Bloomington, Indiana 47403

Dr. K. C. Janda
University of Pittsburg
Chemistry Building
Pittsburg, PA 15260

Dr. E. A. Irene
Department of Chemistry
University of North Carolina
Chapel Hill, North Carolina 27514

Dr. Adam Heller
Bell Laboratories
Murray Hill, New Jersey 07974

Dr. Martin Fleischmann
Department of Chemistry
University of Southampton
Southampton 509 5NH
UNITED KINGDOM

Dr. H. Tachikawa
Chemistry Department
Jackson State University
Jackson, Mississippi 39217

Dr. John W. Wilkins
Cornell University
Laboratory of Atomic and
Solid State Physics
Ithaca, New York 14853

ABSTRACTS DISTRIBUTION LIST, 056/625/629

Dr. R. G. Wallis
Department of Physics
University of California
Irvine, California 92664

Dr. D. Ramaker
Chemistry Department
George Washington University
Washington, D.C. 20052

Dr. J. C. Hemminger
Chemistry Department
University of California
Irvine, California 92717

Dr. T. F. George
Chemistry Department
University of Rochester
Rochester, New York 14627

Dr. G. Rubloff
IBM
Thomas J. Watson Research Center
P.O. Box 218
Yorktown Heights, New York 10598

Dr. Horia Metiu
Chemistry Department
University of California
Santa Barbara, California 93106

Dr. W. Goddard
Department of Chemistry and Chemical
Engineering
California Institute of Technology
Pasadena, California 91125

Dr. P. Hansma
Department of Physics
University of California
Santa Barbara, California 93106

Dr. J. Baldeschwieler
Department of Chemistry and
Chemical Engineering
California Institute of Technology
Pasadena, California 91125

Dr. J. T. Keiser
Department of Chemistry
University of Richmond
Richmond, Virginia 23173

Dr. R. W. Plummer
Department of Physics
University of Pennsylvania
Philadelphia, Pennsylvania 19104

Dr. E. Yeager
Department of Chemistry
Case Western Reserve University
Cleveland, Ohio 41106

Dr. N. Winograd
Department of Chemistry
Pennsylvania State University
University Park, Pennsylvania 16802

Dr. Roald Hoffmann
Department of Chemistry
Cornell University
Ithaca, New York 14853

Dr. A. Steckl
Department of Electrical and
Systems Engineering
Rensselaer Polytechnic Institute
Troy, NewYork 12181

Dr. G.H. Morrison
Department of Chemistry
Cornell University
Ithaca, New York 14853

END

9-87

DTIC